NANOSCOPIC ASPECTS OF RADIOBIOLOGICAL DAMAGE: FRAGMENTATION INDUCED BY SECONDARY LOW-ENERGY ELECTRONS

Léon Sanche*

Group of the Canadian Institutes of Health Research in the Radiation Sciences, Faculté de médecine, Université de Sherbrooke, Sherbrooke (QC), Canada J1H 5N4

Received 25 July 2002; revised 17 October 2002; accepted 18 October 2002

Low-energy electrons (LEEs) are produced in large quantities in any type of material irradiated by high-energy particles. In biological media, these electrons can fragment molecules and lead to the formation of highly reactive radicals and ions. The results of recent experiments performed on biomolecular films bombarded with LEEs under ultra-high vacuum conditions are reviewed in the present article. The major type of experiments, which measure fragments produced in such films as a function of incident electron energy (0.1–45 eV), are briefly described. Examples of the results obtained from DNA films are summarized along with those obtained from the fragmentation of elementary components of the DNA molecule (i.e., thin solid films of H_2O, DNA bases, sugar analogs, and oligonucleotides) and proteins. By comparing the results of these different experiments, it is possible to determine fundamental mechanisms that are involved in the dissociation of biomolecules and the production of single- and double-strand breaks in DNA, and to show that base damage is dependent on the nature of the bases and on their sequence context. Below 15 eV, electron resonances (i.e., the formation of transient anions) play a dominant role in the fragmentation of all biomolecules investigated. These transient anions fragment molecules by decaying into dissociative electronically excited states or by dissociating into a stable anion and a neutral radical. These fragments usually initiate other reactions with nearby molecules, causing further chemical damage. The damage caused by transient anions is dependent on the molecular environment.
 Mass Spec Rev 21:349–369, 2002; Published online in Wiley Interscience (www.interscience. wiley.com). DOI 10.1002/mas.10034
Keywords: *secondary electrons; DNA; oligonucleotides; DNA bases; electron impact; radiation damage; electron-stimulated desorption*

Léon Sanche is Canadian Research Chair in the Radiation Sciences.
Contract grant sponsor: Canadian Institutes of Health Research; Contract grant sponsor: National Cancer Institute of Canada.
**Correspondence to:* Léon Sanche, Group of the Canadian Institutes of Health Research in the Radiation Sciences, Faculté de médecine, Université de Sherbrooke, Sherbrooke (QC), Canada J1H 5N4.
E-mail: Leon.Sanche@USherbrooke.ca

I. INTRODUCTION

High-energy radiation induces damage in liquids and solids *via* the production of intermediate species created within

nanoscopic volumes along ionization tracks (ICRU, 1979; LaVerne & Pimblott, 1995; Cobut et al., 1998). These species consist of excited atoms and molecules, radicals, ions, and secondary electrons. The latter species are created in large quantities ($\sim 4 \times 10^4$ by a 1 MeV particle) and carry most of the energy of the initial fast particle. Secondary electrons have low energies with a distribution that lies essentially below 70 eV and a most probable energy below 10 eV (ICRU, 1979; LaVerne & Pimblott, 1995). At those energies, electrons have thermalization distances of the order of 1–10 nm (Cobut et al., 1998), which define the initial volumes of energy deposition by high-energy radiation. In these volumes, usually called ''spurs,'' the highly excited atomic, molecular and radical species, ions, and low-energy electrons (LEEs) can induce non-thermal reactions within femtosecond times. A majority of these reactive species, which initiate chemical reactions, are created by the secondary electrons. Thus, in order to understand radiation energy deposition processes at the nanoscopic level within condensed matter, the mechanisms of action of LEEs must be known in that phase.

Nanoscopic aspects of the pre-chemical stage of radiation damage can be illustrated by considering the simple example of the initial interaction of a fast charged particle with a molecular solid composed of organic molecules R-H. As the fast charged particle passes near the molecule R-H, that molecule is perturbed by the rapid change of electric field that is induced by the moving charge. Because this perturbation leaves the energy and momentum of the fast particle practically unchanged, the energy transfer can be described as an absorption of electromagnetic radiation by the molecules of the medium (Mott & Massey, 1965; Takayanagi, 1967; Inokuti, 1991). This absorption can lead to the formation of electronically excited species [R-H]*, and ionization (i.e., $[\text{R-H}]^+ + e^-$) as shown in Figure 1 and multiple ionization ($[\text{R-H}]^{n+} + ne^-$) (Inokuti, 1991). The most probable energy loss of fast primary charged particles to produce [R-H]* and ionization is *ca.* 22 eV (LaVerne & Pimblott, 1995; Srdoc et al., 1995). Most of the energy of high-energy particles is, therefore, deposited within irradiated systems by this emission of a succession of low-energy quanta. From the values of the optical oscillator strengths for the dissociative electronic excited states of hydrocarbons (Srdoc et al., 1995), and a comparison with the normalized dipole oscillator strength distribution for DNA and liquid H_2O (LaVerne & Pimblott, 1995), one can estimate that *ca.* 20% of the energy deposited by fast-charge particles in organic matter, including biological and cellular material, leads to [R-H]* production, whereas the rest leads to ionization. The ionization energy is shared as the kinetic energy of secondary electrons and potential energy of the cation,

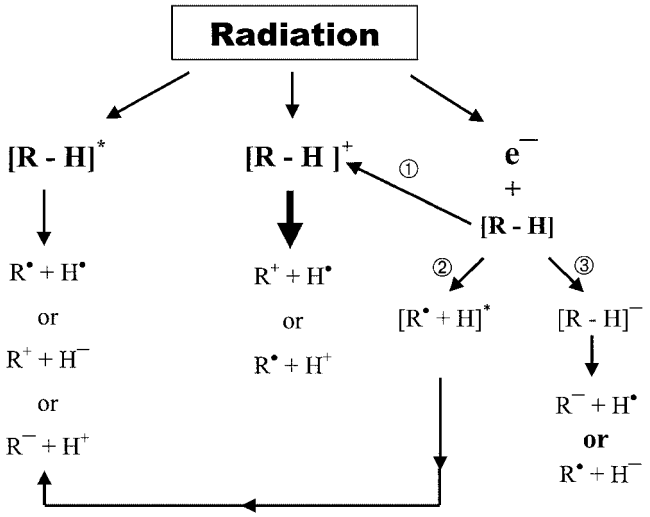

FIGURE 1. Most-probable initial events induced by a fast charged particle that penetrates an organic or bio-organic solid composed of molecules R-H (H = hydrogen, R = rest of molecule). Those events induced by secondary electrons are labeled 1 to 3.

with the largest portion of the energy going to secondary electrons (LaVerne & Pimblott, 1995). The products of ionization and electronic excitation that lead to an hydrogen-atom abstraction are shown in Figure 1, as an example of possible fragmentation produced by ionizing radiation; for simplicity, products that result from multiple ionizations are not shown, but the reaction paths are essentially the same as for single ionization.

A dissociative electronic state [R-H]* can produce two radicals by homologous bond scission or an ion-pair (left vertical arrow in Fig. 1); however, when ionization occurs, the situation is more complex due to the emission of at least one secondary electron. If the positive ion $[\text{R-H}]^+$ is created in a dissociative state, then a cation and a radical can be formed as shown by the larger vertical arrow in Figure 1. The remaining reactions shown in Figure 1 are due to the secondary electron. By interacting with another nearby [R-H] molecule, the secondary electron can produce (Sanche, 1995), depending on its energy, further ionization (pathway 1) and/or dissociation (pathway 2), or it can temporarily attach to a nearby molecule to form a temporary state $[\text{R-H}]^-$, which can subsequently dissociate into the products $R^- + H^\bullet$ or $R^\bullet + H^-$, as shown by the pathway 3 on the rightside of Figure 1. If the temporary state $[\text{R-H}]^-$ is the ground state of the manifold of states of the anion and [R-H] has a positive electron affinity, then the captured electron may permanently stabilize on [R-H] to form a stable anion.

According to the fundamental interactions that lead to the events described in Figure 1, the biological effects

of radiation are not produced by the mere impact of the primary quanta, but rather by the secondary species that are generated along the radiation track (von Sonntag, 1987; Fuciarelli & Zimbrick, 1995). As these species further react within irradiated cells, they can cause mutagenic, genotoxic, and other potentially lethal DNA lesions (Yamamoto, 1976; Ward, 1977). Because LEEs are the most abundant of the secondary species produced by the primary interaction, it is crucial to determine their action within cells, particularly in DNA, where they could induce genotoxic damage. To investigate such damage, experimental efforts have been devoted to isolate biomolecules as thin multilayer films in an ultra-high vacuum (UHV), where they could be bombarded with a beam of LEEs (Klyachko, Huels, & Sanche, 1999; Abdoul-Carime, Dugal, & Sanche, 2000a; Boudaiffa et al., 2000a; Herve du Penhoat et al., 2001; Abdoul-Carime, Cloutier, & Sanche, 2001). Such environmental conditions are necessary to avoid any LEE interaction with small surface impurities, which could modify the probed damage. In these experiments, the fragmentation of biomolecules induced by LEE bombardment can be either analyzed *in situ* or outside UHV. In the former, the mass of the ions and neutral species that desorb from a multilayer film target are analyzed during bombardment (Abdoul-Carime, Dugal, & Sanche, 2000a; Abdoul-Carime, Cloutier, & Sanche, 2001; Herve du Penhoat et al., 2001), or the products that remain in the film are characterized by X-ray photoelectron spectroscopy after bombardment (Klyachko, Huels, & Sanche, 1999). If sufficient degraded material is produced, then the film target can be transported outside the UHV chamber and the products analyzed by standard methods of chemical identification (Boudaiffa et al., 2002).

Recent advances in these techniques have made it possible to measure specific damages to the DNA molecule induced by LEEs (Boudaiffa et al., 2000a). DNA is composed of two strands of repeated sugar-phosphate units hydrogen-bonded together by the bases that are covalently linked to the sugar moiety of the backbone. The short single-strand DNA segment shown in Figure 2b exhibits the repeated sugar-phosphate sub-units of the deoxyribose backbone to which are covalently bonded the bases adenine, cytosine, and thymine (the fourth base guanine is not shown in this example). The results from bombarded plasmid-DNA samples have demonstrated that LEEs can irreversibly damage this backbone by producing single- and double-strand breaks (SSB and DSB), *via* fragmentation of the basic components of the molecule, including its structural water (Boudaiffa et al., 2000a). Investigation of protein fragmentation by LEE impact has also been recently initiated in relation to DNA damage (Abdoul-Carime, Cecchini, & Sanche, 2002). In biological

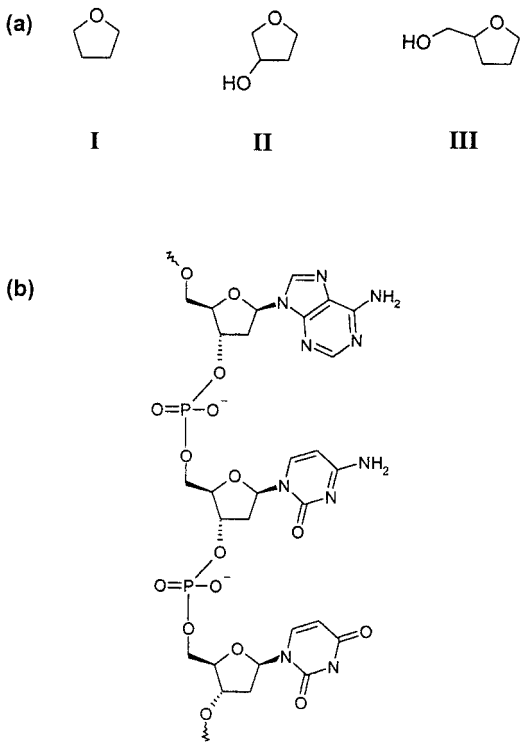

FIGURE 2. (**a**) Schematic drawing of the DNA backbone sugar-like analogs tetrahydrofuran (**I**), 3-hydroxytetrahydrofuran (**II**), and α-tetrahydrofuryl alcohol (**III**). (**b**) A short-chain segment of single-stranded DNA.

cells, nucleic acids interact very closely with certain proteins; some protein components are intercalated within the DNA grooves so that they interact directly with DNA bases (Suzuki, 1990; Werner et al., 1995). After fragmentation of protein subunits by ionizing radiation, the reactive radicals produced may react with a small segment of the nucleic acid and damage the DNA. Thus, understanding radiation and LEE damage to the genome also requires information on damage to proteins.

The results obtained with plasmid DNA and from *in situ* mass analysis of fragments of relevance to DNA damage produced during electron-bombardment of biomolecular films are reviewed in this article. The experimental techniques are briefly explained in the next section, and the background necessary to interpret the data is summarized in Section III. The results obtained from thin films of DNA, water ice, deoxyribose analogs, DNA bases, oligonucleotides, and protein subunits are summarized in Section IV, and specific examples are discussed. The subject of radiosensitivity and its relationship to LEE damage is also treated with pertinent results on bromouracil (BrU) and oligonucleotides.

II. EXPERIMENTAL METHODS

A. Thin-Film Preparation

Depending on the substance to be investigated, the thin films that are to be electron bombarded in an UHV environment must be prepared by different techniques. Gases or liquids, having a significant vapor pressure at room temperature, can be leaked into UHV in front of a cryogenically cooled metal substrate, on which they condense. Those substances that are solids at room temperature can be heated in an oven in front of the metal substrate to produce a flux of molecules that condense on the metal surface. However, if the molecule cannot be heated to sublimate or evaporate without decomposing, then it must be prepared outside the UHV vacuum system in a clean environment.

An apparatus used to measure desorbed neutral species and ion yields from electron-bombarded films of molecules, which form solids at room temperature (Herve du Penhoat et al., 2001), is shown in Figure 3. The UHV apparatus consists of two chambers. The one on the right is a load-lock chamber in which the samples are introduced. It can be pumped to a base pressure in the 10^{-9} Torr range with an oil-free turbomolecular drag-pump station, and it contains a resistively heated oven equipped with an activated shutter. The oven can be transferred into the main chamber on the left (pressure $\sim 10^{-10}$ Torr) for vacuum deposition of the solid compound onto a polycrystalline Pt substrate held at room or cryogenic temperature. The Pt substrate is fixed to a rotatable sample holder in order to place the target in front of the electron gun and mass spectrometer.

Once loaded into a miniature oven, the sample to be investigated is degassed by heating for several hours well below its evaporation temperature. The evaporation-rate dependence on oven temperature is determined in the load-lock chamber by recording the partial pressure of the molecules with a residual-gas analyzer as a function of oven temperature (Herve du Penhoat et al., 2001). Once the oven has reached evaporation temperatures, it is transferred into the main chamber and is placed at *ca.* 1 cm from the sample holder; subsequently, the shutter is opened, and compounds are thermally evaporated onto the polycrystalline Pt substrate. The latter is clamped to, but electrically isolated from, the rotatable sample holder, which can be cooled by a cryostat. The substrate is cleaned prior to each deposition by resistive heating. The integrity of the sublimated films can be verified *in situ* by X-ray photoelectron spectroscopy (Klyachko, Huels, & Sanche, 1999) and outside of the vacuum by chromatography. The average film thickness is determined within 50% accuracy by measuring the mass of the condensed film with a quartz crystal microbalance.

Volatile compounds can be introduced directly into the main chamber *via* a tube that ends in front of the Pt substrate. This tube is connected to a valve that allows the gas or vapor, contained at a known pressure in a calibrated volume, to expand into vacuum. In this case, the metal substrate must be cooled to cryogenic temperatures

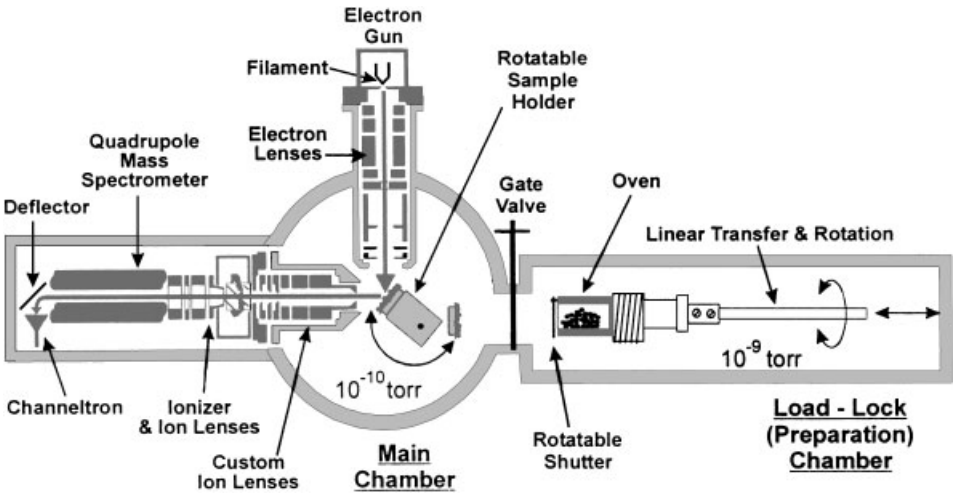

FIGURE 3. Schematic overview of the type of apparatus used to investigate the desorption of ions and neutral species induced by electron impact on thin molecular and bio-organic films. The thin films are usually formed by the condensation of molecules evaporated from an oven or leaked in front of a metal substrate fitted to the rotatable sample holder. (Reprinted with permission from Herve du Penhoat et al. [2001]. Copyright 2001 American Institute of Physics.)

(15–100 K) in order to avoid substantial evaporation of the film in UHV. The film thickness can be estimated to within a 20–50% accuracy from gas-volume expansion and by measuring the thickness-dependence of the electron current transmitted through the film during the experiment (Sanche, 1991).

For compounds that might be destroyed by evaporation into vacuum, two different techniques have been developed to produce thin biomolecular films on metal substrates. When multilayer films are required, a solution of the compound is made and a small aliquot of the solution is lyophilized on a tantalum substrate (Boudaiffa et al., 2002). The sample preparation and manipulations are performed within a sealed glove box under a pure dry-nitrogen atmosphere. Several samples are afterwards transferred directly into an UHV system, or *via* a load-lock—as shown in Figure 3. Samples are placed on a rotary multi-sample holder, which can transport each sample in front of the LEE beam. The average film thickness is usually estimated from the amount deposited and the density (Boudaiffa et al., 2002).

It has been shown that, upon adsorption onto a metal surface, certain biomolecules may chemically decompose (Patthey, 1995; Nyberg et al., 2000). For instance, glycine fragments into CH_3/NH_2 and CO_2 when adsorbed onto a Cu (110) surface (Nyberg et al., 2000). Such chemical decomposition may also occur on other metal substrates. Therefore, relatively thick ($\sim$5 ML) monolayer films are usually deposited to insure that the measured signal arises from electron interaction with biomolecules that lie close to the film-vacuum interface.

When only a single layer of a relatively large biomolecule is needed, a uniform layer can be formed on a gold substrate by chemisorption if the molecule does not fragment on the metal. The technique is essentially the same as that utilized to prepare self-assembled monolayers (Porter et al., 1987; Dugal, Huels, & Sanche, 1999). It has served to prepare films of oligonucleotides that consist of six to twelve bases (e.g., a trimer is shown in Figure 2b). However, compared to self-assembled monolayers, the large biomolecules are not necessarily well ordered on the substrate. The gold substrate is usually prepared by vacuum evaporation of high-purity gold (99.9%) onto freshly cleaved preheated mica slides (Dugal, Huels, & Sanche, 1999). These slides are dipped for at least 24 h in an aqueous solution of highly purified oligonucleotides. With this procedure, one monolayer (Dugal, Huels, & Sanche, 1999; Dugal, Abdoul-Carime, & Sanche, 2000) is chemically anchored to the gold substrate *via* the phosphotioate modification on each deoxycytosine nucleotide (i.e., substitution of the double-bonded oxygen atoms by double-bonded sulfur at the phosphorus). In this surface configuration, the oligos are expected to lie parallel to the gold surface with the DNA bases facing vacuum. Considering that the chemisorbed oligos are well ordered and densely packed, an upper limit for the DNA bases surface coverage (i.e., $N_0 \approx 1.7 \times 10^{14}$ bases/cm^2) (Abdoul-Carime, Dugal, & Sanche, 2000a) is obtained, regardless of the nature and number of the bases. The reproducibility of the results obtained so far (Dugal, Huels, & Sanche, 1999; Dugal, Abdoul-Carime, & Sanche, 2000; Abdoul-Carime, Dugal, & Sanche, 2000a) suggests that the surface coverage is constant within 20% of the data spread. After removal of the mica-Au-oligo slide from the solution, it is rinsed with a copious amount of nanopure water and dried under nitrogen flow. Each slide is divided into smaller samples, which are afterwards mounted on a rotary multiple sample holder and introduced in a UHV preparation chamber for *ca.* 12 h of degassing. The oligonucleotides are free of the hydration layer, but a small amount of ''structural'' water is likely to remain tightly bound to the oligos. Afterwards, the eight samples are transferred from the load-lock chamber to the main chamber, *via* a gate valve as shown in the schematic diagram of Figure 3.

B. Electron-Stimulated Desorption (ESD) of Ions and Neutral Species

Some of the damage induced by LEE impact on biomolecular films can be assessed by monitoring the ions and neutral species that desorb in vacuum, while the film is being bombarded. Such measurements can be performed by placing the sample near a mass spectrometer—as shown in Figure 3. A LEE beam, emanating from an electron monochromator or a focusing electron gun, impinges onto the sample. In certain systems, the focused electron beam ($\approx$ 3-mm diameter spot) can be displaced across the sample surface by two sets of orthogonal electrostatic deflector plates. The full-width at half-maximum of the electron-energy distribution varies from 0.03 to *ca.* 0.3 eV, depending on the type of electron source for typical beam currents of 5–400 nA. The incident electron-energy scale is calibrated such that 0 eV corresponds to the onset of electrons transmitted to the metal substrate (Sanche & Deschênes, 1988) (i.e., 0 eV is defined as the vacuum level). This onset can be determined within an accuracy of $\pm$ 0.25 to $\pm$ 0.05 eV. Because energy shifts in this onset are related to electron trapping, this method allows one to verify that measurements are obtained from uncharged films; alternatively, with this method it is possible to obtain an estimate of charge accumulation during electron impact (Marsolais, Deschênes, & Sanche, 1989). Although relatively high currents were required to detect desorption of certain fragments in the experiments reported in this review, no charging was detected within the stated accuracy in energy scale.

Neutral species desorbed from the films that reach the ionizer of the mass spectrometer, shown in Figure 3, can

be ionized and focused onto the quadrupole rods. Charged particles are kept from reaching the ionizer by placing suitable potentials on grids or lenses located between the target and the ionizer. To increase the detection efficiency of desorbing neutral species, the latter can be ionized close to the target surface by a laser (Kimmel & Orlando, 1995). With a standard electron-ionization source, the background signal can be discriminated by beam modulation lock-in techniques (Rakhovskaia, Wiethoff, & Feulner, 1995). Such measurements do not allow the determination of absolute yields.

In order to determine the absolute desorption yields of neutral products, their formation must be related to a pressure rise within a relatively small volume. In this case, a mass spectrometer measures the partial-pressure increase in a small UHV chamber due to the desorption of a specific fragment induced by LEE impact on a thin film (Dugal, Huels, & Sanche, 1999; Dugal, Abdoul-Carime, & Sanche, 2000; Abdoul-Carime, Dugal, & Sanche, 2000a). At equilibrium, the number of fragments desorbed per unit time, $N_d/\Delta t$, is equal to the partial pressure variation, ΔRPP, times a factor of 1.3×10^{18} that corresponds to SN/RT, where S is the true nominal pumping speed of the system, N is Avogadro's number, R is the perfect gas constant, and T is the temperature (Dugal, Abdoul-Carime, & Sanche, 2000). The effective number of a specific fragment desorbed per incident electron is proportional to the effective desorption cross-section *via* the constant (N_0/a), where N_0 is the initial number of target molecules in the irradiated area a (Dugal, Abdoul-Carime, & Sanche, 2000; Abdoul-Carime, Dugal, & Sanche, 2000b).

As shown in Figure 3, ions that emerge from the film can be focused by ion lenses located in front of the mass spectrometer. For such measurements, the ionizer of the mass spectrometer is turned off. In certain systems, grids are inserted between the lenses in order to analyze the ion energies by the retarding-potential method. Relative ion yields can be obtained from three different operating modes (Sanche, 1995): (1) the ion-yield mode, in which ions of a selected mass are detected as a function of incident electron energy, (2) the ion-energy mode, in which the ion current at a selected mass is measured for a fixed electron energy as a function of the retarding potential, and (3) the standard mass mode, in which the intensity of mass peaks is measured for a fixed electron energy.

C. Analysis by Electrophoresis

Once extracted from vacuum, the irradiated samples can, in principle, be identified by various standard methods of chemical analysis. In practice, however, the quantity of recovered material and fragments are so small that an efficient method of damage amplification is required to observe any type of fragmentation. One method of damage amplification consists of using a target film, in which a small modification at the molecular level can cause a large conformational change. As far as biomolecular films are concerned, only strand breaks in supercoiled DNA have so far been investigated with such a method. In this case, a single bond rupture in a plasmid of a few thousand base pairs (bp) can cause a conformational change in the geometry of DNA, and hence be detected efficiently by electrophoresis.

The DNA experiments were performed by Boudaiffa et al. [2000a,b, 2002] and Huels et al. (submitted), who bombarded, with 3 eV to 1.5 keV electrons, pure dry samples of supercoiled DNA under a hydrocarbon-free 10^{-9} Torr residual atmosphere. Plasmid DNA [pGEM 3Zf(−), 3,199 bp] was first extracted from *Escherichia coli* DH5α, purified, and resuspended in nanopure water without any salt. Dry DNA films were formed in a clean N_2-filled glove box: an aliquot of the pure aqueous DNA solution was deposited onto chemically clean tantalum substrates held at liquid nitrogen temperature, lyophilized with a hydrocarbon-free sorption pump at 0.005 Torr, and transferred directly into a UHV chamber without exposure to air. After evacuation for ~24 h, the room-temperature DNA solid films, of 5 monolayer (ML) average thickness and 6 mm diameter sample, still contained 2.5 H_2O molecules/bp as structural water (Boudaiffa et al., 2002). Each target film was bombarded with a monochromatic LEE beam of the same diameter, for a specific time at a fixed beam current density (2.2×10^{12} electrons s^{-1} cm^{-1}) and incident electron energy. After bombardment, the DNA was analyzed by agarose gel electrophoresis and quantified as supercoiled (undamaged), nicked circle (SSB), full-length linear (DSB), or short linear forms (Boudaiffa et al., 2000a, 2002). The procedure was repeated at different electron energies and periods of bombardment.

III. INTERPRETATION OF THE DEPENDENCE OF ION AND NEUTRAL YIELDS ON INCIDENT ELECTRON ENERGY

In order to interpret in terms of fundamental processes the incident-energy dependence of the yields of fragments (i.e., the yield functions) induced by LEE impact on biomolecular films, some knowledge of the basic interaction between an electron and a molecule is required. In general, the interaction of an electron with an atom or a molecule can be described in terms of forces derived from the potential that acts between them. There are basically three types of forces between an electron and a molecule (Mott & Massey, 1965): (1) the electrostatic force, which acts between the projectile electron and the constituent-charged elementary particles of the target; (2) the exchange force, which reflects the requirement that the electron-target

system wave function must be antisymmetric under pairwise electron interchange; and (3) the induced polarization attraction, which is due to the distortion of the target orbitals by the electric field of the projectile electron. Forces (1) and (3) can be described by a potential that consists of a series of terms, whose magnitude depends on electron energy (Takayanagi, 1967). At high energies, the dipole term dominates the interaction, but as the energy falls below *ca.* 1 keV, other terms may become important (e.g., those that involve the quadrupole and higher moments), depending on momentum transfer. At even lower energies, particularly below 30 eV, the scattering electron can modify molecular orbitals, giving rise to induced-polarization interaction (Mott & Massey, 1965; Massey, 1976). Furthermore, at such low energies, the exchange force becomes more effective, and it must be taken into account in the electron-molecule potential. At certain energies, the forces that act between an electron and a molecule may combine to produce an effective potential capable of momentarily capturing the scattering electron. This ''resonance'' phenomenon causes the formation of a transient anion (Schulz, 1973).

The electron–molecule interaction at low energies (1–30 eV) can, therefore, be described in terms of resonant and non-resonant or direct scattering. The latter occurs at all energies above the energy threshold for the observed phenomenon, because the potential interaction is always present. Thus, direct scattering produces, in low-energy yield functions, a smooth usually rising signal that does not exhibit any particular features. However, resonance scattering occurs only when the incoming electron occupies a previously unfilled orbital of the molecule. Such an orbital exists at a precise energy (Allan, 1989; Sanche, 1991), and thus, resonance scattering occurs only at specific energies that correspond to the formation of transient anions. At the resonance energy, product yield is usually enhanced, and a strong peak is observed in the yield function. The dependence of the desorbed ion and neutral yields on incident-electron energy is, therefore, expected to exhibit pronounced maxima superimposed on an increasing monotonic background that results from direct scattering.

Electron resonances are well described in the literature and many reviews contain information relevant to this scattering phenomenon (Schulz, 1973; Massey, 1976; Christophorou, 1984; Allan, 1989; Sanche, 1991, 1995, 2000; Palmer & Rous, 1992). There are two major types of resonances or transient anions (Schulz, 1973). If the additional electron occupies a previously unfilled orbital of the target in its ground state, then the transitory state is referred to as a single-particle or ''shape'' resonance. The term ''shape'' resonance applies more specifically when temporary trapping of the electron is due to the shape of the electron-molecule potential. When the transitory anion is formed by two electrons that occupy previously unfilled orbitals, the resonance is called ''core-excited'' and may be referred to as a two-particle, one-hole state.

For a simple molecular liquid or solid composed of diatomic molecules, AB, unimolecular fragmentation pathways at low energies are described in Figure 4. The direct electron interaction may produce an excited neutral state of the molecule (AB*) *via* pathway a. AB* may dissipate its excess energy *via* photon emission and/or energy transfer to the surrounding medium (i.e., a1). If the configuration of an electronically excited state is dissociative, then AB* may dissociate into two atoms (or neutral radicals in the case of a more complex molecule) as shown by the a2 pathway. Above a certain energy threshold (~14–16 eV), fragmentation *via* dipolar dissociation (DD), path a3, becomes possible to yield an anion and a cation. In the case of resonant scattering, the incident electron temporarily attaches to the molecule *via* the b pathway. The resulting transient anion may autoionize *via* b2 or, for a sufficiently long-lived anion in a dissociative state, it may fragment into a stable anion and a neutral atom or radical, (i.e., b1); this latter mechanism is known as dissociative electron attachment (DEA). When the $(AB^-)^*$ state lies above the energy of the first electronically excited state of AB, the molecule can be electronically excited after

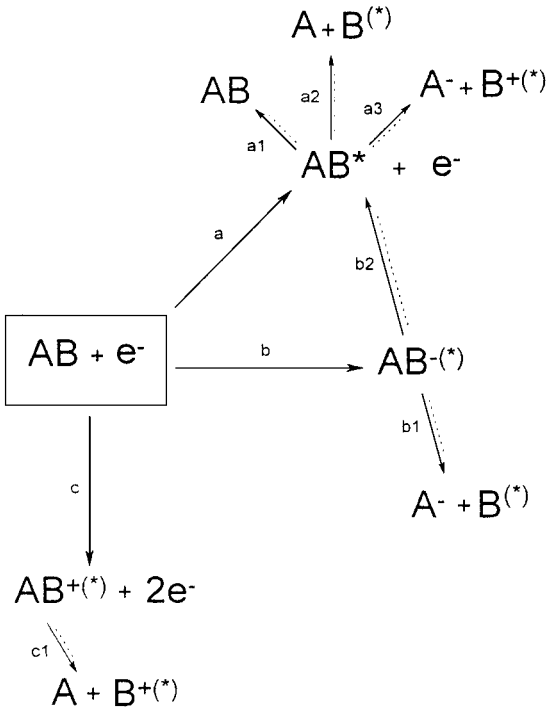

FIGURE 4. Energy transfer and unimolecular fragmentation pathways that follow low-energy electron interaction with a molecule AB. The asterisk in parentheses indicates that the species could be electronically excited. (Reprinted with permission from Dugal et al. [2000]. Copyright 2000 American Chemical Society.)

electron detachment (b2); in this case, it could decay into the a1, a2, and a3 pathways previously described. Finally, the incoming electron can directly ionize the molecule *via* path c, and if the resulting cation is dissociative, then it may fragment, as shown by reaction c1. This dissociation channel is usually non-resonant.

IV. RESULTS AND DISCUSSION

A. Desorption of Ions and Neutral Species from Water-ice Films Induced by Low-Energy Electrons (LEEs)

Some of the damage induced by low-energy electron impact on amorphous ice films has been measured by recording H^- (Rowntree, Parenteau, & Sanche, 1991; Simpson et al., 1997, 1998), H_2 (Kimmel et al., 1994; Kimmel & Orlando, 1996), $D(^2S)$, $O(^3P)$, and $O(^1D_2)$ (Kimmel & Orlando, 1995; Kimmel et al., 1997) desorption-yield functions in the range 5–30 eV. Most of these functions exhibit resonance structures below 15 eV, which are characteristic of transient anion formation. From anion yields, DEA to condensed H_2O (pathway b → b1 in Fig. 4) was shown to result principally in the formation of H^- and the $OH^\bullet$ radical from dissociation of the $^2B_1$ state of H_2O^- located in the 7–9 eV region. Figure 5 exhibits the H^- ESD yield function that results from the dissociation of the $^2B_1$ state and smaller contributions from the $^2A_1$ and $^2B_2$ anionic states, which are formed near 9 and 11 eV, respectively (Rowntree, Parenteau, & Sanche, 1991; Simpson et al., 1997)]. At higher energies, non-resonant processes, such as DD (pathway a → a3 in Fig. 4), lead to H_2O fragmentation with the assistance of a broad resonance that extends from 20 to 30 eV (Simpson et al., 1997). This higher-energy resonance is clearly seen in the yield of neutral molecular hydrogen recorded by Kimmel & Orlando (1996).

In some of the water-ice experiments, the temperature of the substrate was modified before or after water condensation in order to investigate the effects of morphology and porosity (Simpson et al., 1997, 1998). The electron-energy dependence of the D^- signal from 20 bilayers of porous amorphous ice, grown at 27 K (Simpson et al., 1998) and recorded at various film temperatures, is shown in Figure 5. The resonance energies and the anionic yields both change with temperature. An analysis of the D^- onset energy and the energy and intensity of the resonance peak indicates that there is a break in this behavior at *ca.* 60 K. The peak intensity increases fivefold between 27 and 60 K, remains *ca.* constant between 60 and 100 K, and more than doubles between 100 and 140 K. These results were attributed to the thermally induced movement of the hydrogen-bonding network, which changes the orientation of the surface molecules and the lifetimes of the predissociative transient anions that lead to the ESD of D^-.

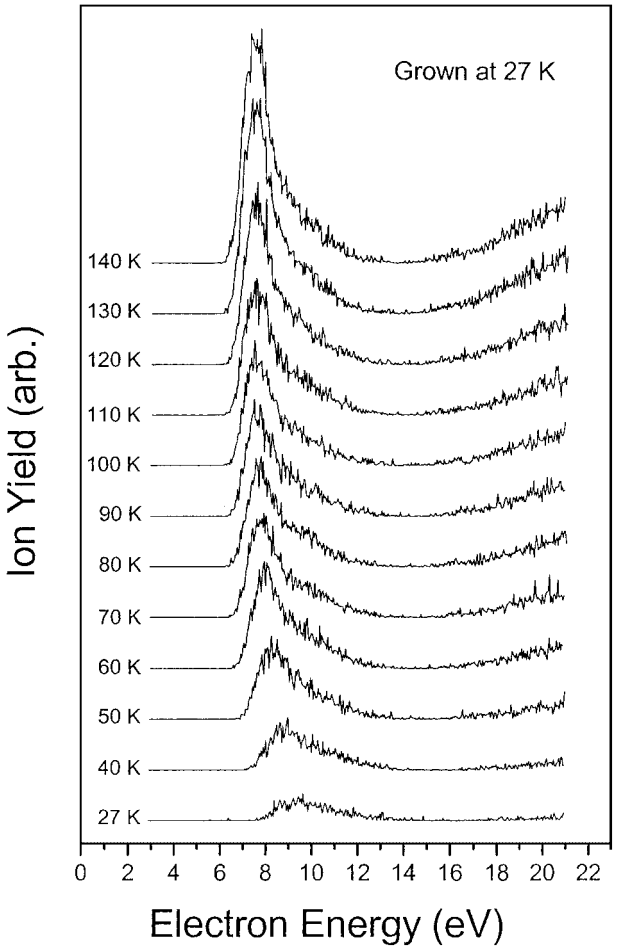

FIGURE 5. D^- signal desorbed by the impact of 3–21 eV electrons from 20-bilayer porous amorphous ice films grown at 27 K and raised to various temperatures. Individual scans are offset vertically for display, and are labeled with the temperature at which they were recorded. (Reprinted with permission from Simpson et al. [1997]. Copyright 1997 American Institute of Physics.)

Kimmel et al. measured the D_2 ($X^1\sum_{g+}$), $D(^2S)$, $O(^3P_{j=2,1,0})$, and $O(^1D_2)$ products (Kimmel & Orlando, 1995; Kimmel et al., 1997) that desorb from D_2O multilayers (~20 nm) grown on a platinum (111) crystal at 88 K under conditions that are known to produce amorphous ice. The ice samples were irradiated with a pulsed electron beam in an apparatus similar to the one shown in Figure 3 and the desorbing neutral products were ionized by laser resonance-enhanced multiphoton absorption. State-specific time-of-flight distributions were obtained by varying the delay time between the electron-beam pulse and the laser pulse. The $D(^2S)$, $O(^3P_2)$, and $O(^1D_2)$ yields versus incident electron energy are shown in

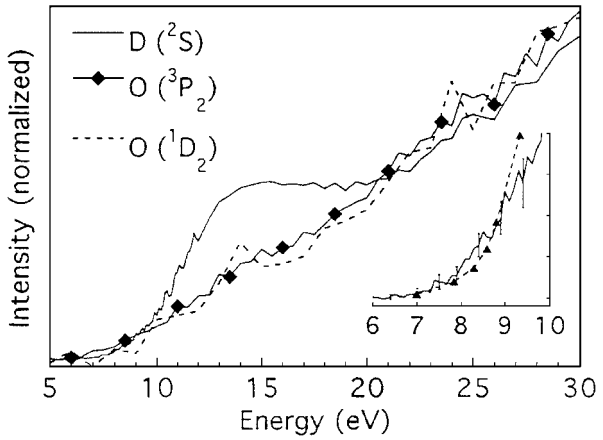

FIGURE 6. Stimulated desorption from amorphous ice of the atoms D(^{2}S), O(^{3}P$_2$), and O(^{1}D$_2$) vs. incident electron energy. The D(^{2}S) yield rises rapidly above threshold, and is constant from ~14 to 20 eV. The O(^{1}D$_2$) and O(^{3}P$_2$) signals have a similar threshold, but increase linearly above threshold. The scatter in the data is indicative of the statistical error. (Reprinted with permission from Kimmel and Orlando, Phys Rev Lett, 75: 2606–2609 [1995]. Copyright 1995 by the American Physical Society.)

Figure 6. The spectra were obtained with electron-beam pulse-widths that integrate the entire velocity distributions. The D(^{2}S) has an apparent threshold at ~6.5 eV. Above this threshold, the D(^{2}S) intensity increases rapidly until a distinct plateau is reached for $\sim 14 \leq \mathrm{Ei} \leq 21$ eV. The signal increases more gradually for electron energies above $\gtrsim$ 21 eV. The thresholds for the O(^{3}P$_2$) and O(^{1}D$_2$) signals lie in the range 6–7 eV. Whereas the O(^{3}P$_2$, ^{1}D$_2$) yields arise exclusively from direct electron-molecule scattering (pathways a → a2 in Fig. 4), the broad peak located near 14 eV in the D(^{2}S) yield function could arise from a superposition of a contribution from resonance scattering *via* the pathways b → b2 → a2 shown in Figure 4 and direct scattering. However, this structure observed in the D-atom yield has been attributed mainly to ionization (Kimmel & Orlando, 1995) near the surface, leading to exciton formation by electron-ion recombination. D-atom desorption then occurs from exciton dissociation.

The low threshold energies for the production of D(^{2}S), O(^{3}P), and O(^{1}D$_2$) show the importance of valence-excited states in the ESD of neutral fragments (Kimmel & Orlando, 1995). The pathway for D(^{2}S) desorption involves $D_2O^* \rightarrow D^\bullet + OD^\bullet$, but the thresholds to produce O(^{3}P$_2$) and O(^{1}D$_2$), which are the same within experimental error, are lower than the 9.5 and 11.5 eV thermodynamic energies required to produce O(^{3}P$_2$) + 2D(^{2}S) and O(^{1}D$_2$) + 2D(^{2}S), respectively. The low threshold values, therefore, indicate that the formation of O(^{3}P$_2$) and O(^{1}D$_2$) must occur by a pathway that involves the simultaneous formation of D_2. Kimmel et al. (1994) have in fact reported a threshold for the production of D_2 from D_2O ice at ~6–7 eV that supports this conclusion. Above the ionization threshold of amorphous ice, these excited states can be formed *via* pathways a → a2, b → b2 → a2, or c → c1, shown in Figure 4, or *via* electron-ion recombination.

The desorption of hydrogen and deuterium cations induced by LEE impact on 1–40-ML film of H_2O and D_2O, respectively, has been reported by many authors (Stockbauer et al., 1982; Rosenberg et al., 1983; Ding et al., 1984; Bertel et al., 1985; Noell, Melius, & Stulen, 1985; Stulen & Thiel, 1985; Bennett et al., 1991; Sieger, Simpson, & Orlando, 1997, 1998). The energy dependence of the total yield and the velocity distribution were recorded by Sieger, Simpson, & Orlando (1997) as a function of film thickness, temperature, and ice phase from 90 to 200 K. The D^+ yields were found to change as a function of these parameters. The total D^+ ESD yields as a function of electron energy from 40 ML amorphous and crystalline D_2O ice films, respectively, at two representative temperatures (Sieger, Simpson, & Orlando, 1997) are shown in Figure 7. Two major thresholds are evident: A at ~22–24 eV and B at ~40 eV. Threshold A has been assigned to deep-valence excitation followed by a shake-up to two-hole-one-electron (2h1e) dissociative excited states, (Noell, Melius, & Stulen, 1985; Stulen & Thiel, 1985; Bennett et al., 1991). Threshold B has been tentatively assigned to valence excitation plus shake-off to form two-hole (2h) states, which dissociate *via* a Coulomb explosion (Rosenberg et al., 1983; Ding et al., 1984; Bertel et al., 1985; Stulen & Thiel, 1985). The insets show the onset of emission at low and high temperatures. The onset for desorption from crystalline ice appears to shift by almost +2 eV between 110 and 155 K, whereas the amorphous ice shows a smaller shift. This shift in threshold energy could not be accounted for (Sieger, Simpson, & Orlando, 1997) by the temperature dependence of the work function (Langenbach, Spitzer, & Luth, 1984). Instead, it appeared that an excitation channel is being suppressed for high-temperature crystalline ice.

Detailed measurements indicated that the D^+ yield generally increases with temperature, rising to near 120 K on amorphous ice, and to near 135 K on crystalline ice. An amorphous-crystalline phase transition at ~160 K was found to cause a drop in the total desorption yield. The temperature dependence of D^- desorption *via* the $^2B_1$ dissociative electron attachment resonance shown in Figure 5 is very similar to that of the D^+ yield measured by Sieger et al. (1997) and likely involves similar restructuring and lifetime effects. However, no electron-resonance structures have been observed so far in any of the ESD yield function of cations. The anion and cation data from water-ice films collectively suggest that a thermally activated reduction of surface hydrogen-bonding increases the lifetime of the excited states that are responsible for ion

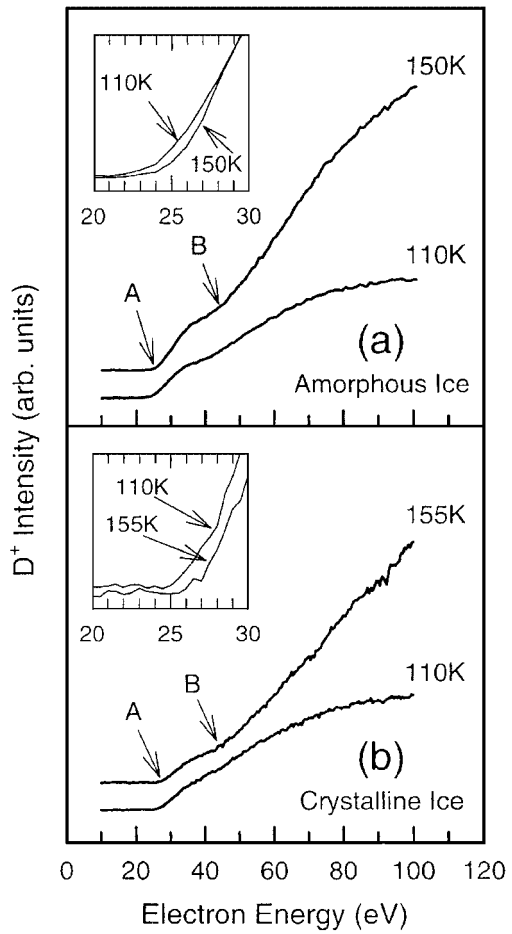

FIGURE 7. Total D^+ yield desorbed by 20–100 eV electrons recorded at different temperatures from 40 monolayer (ML) films of (**a**) amorphous ice and (**b**) crystalline ice. The curves are offset for clarity. The thresholds are labeled A and B. Insets show near-threshold behavior as a function of temperature. These results were taken from Seiger, Simpson, and Orlando, Phys Rev B, 56:4925–4937 (1997). Copyright 1997 by the American Physical Society. Reproduced with permission.

desorption, and that these lifetime effects are strongest for excited states that involve a_1 bands (Sieger, Simpson, & Orlando, 1997).

B. Anion ESD from Thin Films of Deoxyribose Analogs

As shown in Figure 2, tetrahydrofuran and its analogs (i.e., compounds **I**, **II**, and **III**) are part of the basic molecular sub-units of the DNA backbone. In DNA, a single-strand break occurs when one of the two backbones is broken. If breaks occur on two chains within a short distance (~10 bp or 30 Å), then the damage is referred to as a double-strand break. To understand how such breaks can occur *via* LEE impact on specific sub-units of the backbone, ESD experiments were performed with solid films of the sugar-like analogs, tetrahydrofuran (**I**), 3-hydroxytetrahydrofuran (**II**), and α-tetrahydrofuryl alcohol (**III**) (see Fig. 2).

The yields of H^- ion desorbed by the impact of 1–20 eV electrons on 10-ML film of **I**, **II**, and **III** are shown in Figure 8. The curves are characterized by an onset at 6.0, 5.8, and 6.0 eV, respectively and a yield maximum centered at 10.4, 10.2, and 10.0 eV for **I**, **II**, and **III**, respectively. Other weaker features are also observed in the H^- yield functions for **II** and **III**; they appear on the low-energy side of the 10 eV peak. These results were generated by measuring, with an experimental arrangement of the type shown in Figure 3, the H^- anions desorbed by a collimated 4 nA electron beam of 80 meV full-width at half-maximum, incident at an angle of 70° from the surface normal of the sample film (Antic et al., 1999). The multilayer films of **I**, **II**, and **III** were grown in UHV on an electrically isolated polycrystalline platinum ribbon attached to the tip of a closed-cycle helium-refrigerated cryostat (Antic et al., 1999).

All features below 15 eV in Figure 3 are characteristic of DEA to **I**, **II**, and **III**. The steep rise in the H^- signal with

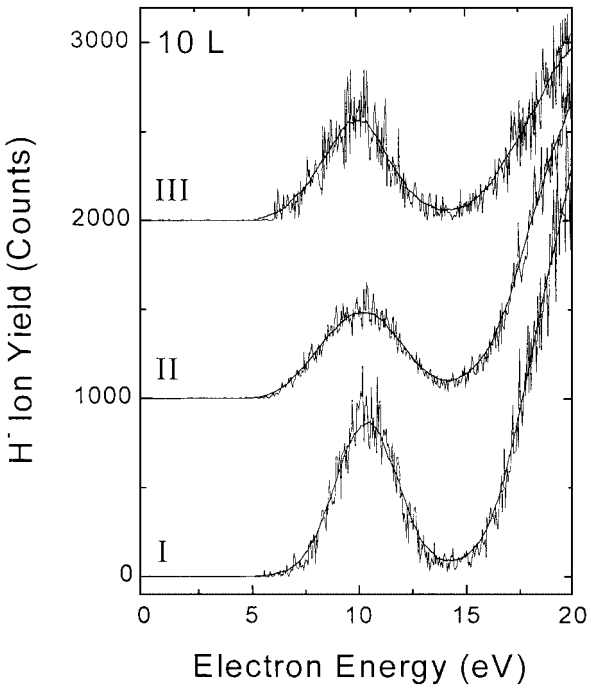

FIGURE 8. H^- desorption yields stimulated by the impact of 1–20 eV electrons on 10-ML thick films (10 L) of compounds **I**, **II**, and **III**, whose chemical structures are shown in Figure 2. The smooth solid-lines serve as guides to the eye, and the "zero-count" baselines have been shifted vertically for clarity in the case of compounds **II** and **III**. (Reprinted with permission from Antic et al. [1999]. Copyright 1999 American Chemical Society.)

an energetic threshold near 14.5 eV is characteristic of non-resonant DD of C-H bonds in **I**, **II**, and **III**; it could also partially arise from DD of the O-H bond in **II** and **III**. The formation of H^- *via* DEA from **I**, **II**, and **III** has been discussed in detail by Antic et al. (1999). These authors considered the possibility that H^- arise from dissociation of the tetrahydrofuran ring, and of the $-OH$ and the $-CH_2OH$ groups. Other decay channels of the transient anions could result in the formation of larger anion fragments, such as OH^- and CH_2OH^-, and could compete with H^- production; however, these heavier ions were not observed to desorb. Typically, large-mass fragments do not possess sufficient kinetic energy to escape the induced polarization, and thus they remain trapped within the film or at its surface (Huels et al., 1995). Owing to the strong similarity of the H^- desorption profiles for **I**, **II**, and **III**, those authors concluded that the majority of the anion yield for all three systems arises from at least one transient anion associated with electron attachment to the furan ring and located near 10 eV. Considering the large Rydberg character of the excited states in **I** near the energy range of the observed resonance, they further suggested that this resonant state is of the core-excited type, possibly with dissociative valence σ^* configurational mixing.

C. Anion ESD from Thin Films of DNA Bases

Electron-impact dissociation of DNA bases and halogen-substituted bases has been investigated in the gas- and condensed-phases (Huels et al., 1998; Klyachko, Huels, & Sanche, 1999; Herve du Penhoat et al., 2001; Abdoul-Carime, Cloutier, & Sanche, 2001). In both phases, a large variety of stable anions is produced *via* DEA to the bases for electron energies below 30 eV. The anions H^-, O^-, CN^-, CH_2^-, OCN^-, and $OCNH_2^-$ were observed from gaseous thymine, whereas electron impact of gaseous cytosine resulted in the formation of the anions H^-, C^-, O^- and/or NH_2^-, CN^-, OCN^-, $C_4H_5N_3^-$ and/or $CH_4N_3O^-$, and $C_3H_3N_2^-$ (Abdoul-Carime et al., 2001).

All four bases were investigated in the form of thin multilayer films, but fewer anions of different masses were measured than in the gas phase. The difference is principally due to the inability of the heavier anions to overcome the polarization potential that they induce in the film (Huels et al., 1995), causing them to remain undetected in the target. In fact, only the light anions H^-, O^-, OH^-, CN^-, OCN^-, and CH_2^- were found to desorb by the impact of 5–35 eV electrons on physisorbed adenine, thymine, guanine, and cytosine *via* either single or complex multibond dissociation (Abdoul-Carime, Cloutier, & Sanche, 2001). The H^- yield functions produced by 5–45 eV electron impact on thin films of adenine and thymine are shown in Figure 9a,b, respectively. The functions presented in c and d were obtained by subtracting, from the curves in a and b, respectively, a background signal that rises linearly with the electron energy and has a threshold at 10 eV. The results of Figure 9 were obtained from an irradiation of 1–10-ML films by a 6 nA electron beam. The yield functions of H^- ions desorbed by electron impact on guanine and cytosine films exhibit the same electron-energy dependence as that shown in Figure 9. The H^- yield function exhibits resonance structures at around 9 and 20 eV, which are typical signatures of DEA to the molecule. The subtracted monotonic increase of the ion yield represents a non-resonant stable-anion production *via* DD (i.e., pathway $a \rightarrow a3$ in Fig. 4: direct scattering of the electron without attachment to the molecule). The resonance features may be compared with the structures reported earlier in electron energy-loss spectra (Crewe, Isaacson, & Johnson, 1971; Dillon, Tanaka, & Spence, 1989) and ultraviolet photoelectron (Yu et al., 1978) studies of nucleic acid bases. According to theoretical *ab initio* calculations (Mely & Pullman, 1969; Lorentzon, Fulsher, & Roos, 1995), transient anion formation at 8–9 and 14–15 eV can be attributed to electron capture by the positive electron-affinity of excited states that involves the excitation of the lone-pair $n \rightarrow \pi^*$, $\pi \rightarrow \pi^*$, and/or $\sigma \rightarrow \sigma^*$ (i.e., formation of a two-electron one-hole transitory anion). Thus, the formation of H^- at these energies is likely to occur through a dissociation of a core-excited resonance ($b \rightarrow b1$ in Fig. 4). Moreover, according to the previous work on gas-phase deuterated thymine (Huels et al., 1998), the H^- peak at 9 eV would arise from a C-H bond cleavage.

The origin of the peak at around 20 eV in Figure 9 is less obvious because it lies well above the DD threshold. Beyond 12 eV, resonance features may arise from DEA ($b \rightarrow b1$ in Figure 4) or from the decay of the transitory anion into the DD continuum ($b \rightarrow b2 \rightarrow a3$ in Fig. 4; e.g., for thymine, $e + T \rightarrow T^- \rightarrow T^* + e \rightarrow \text{radical}^+ + H^- + e$). Higher-energy features may also arise from energy losses prior to DEA (Antic, Parenteau, & Sanche, 2000; Hoffman et al., 2001). Thus, the 20-eV peak in Figure 9 could also contain contributions from electrons that lose ~11 eV and form the dissociating 9-eV anion state.

Another example of anion ESD from thin films of DNA bases is provided in Figure 10. This figure exhibits the CN^- yield functions produced by 3–20 eV electrons that impinge on thin films of each one of the four bases. The maxima in the yield functions are characteristic of DEA to the bases. Whereas H^- ion desorption, such as that shown in Figure 9, can be induced *via* a simple bond cleavage from the bases, the production of CN^- occurs under a more complex ring-dissociation. From the structure of the DNA bases (Fig. 2), it can be readily seen that the extraction of a CN^- anion must involve more than a single bond cleavage. In other words, during the lifetime of the negative ion, not only does exocyclic single bond cleaveage occurs, but also complex endocyclic multibond cleavages are involved

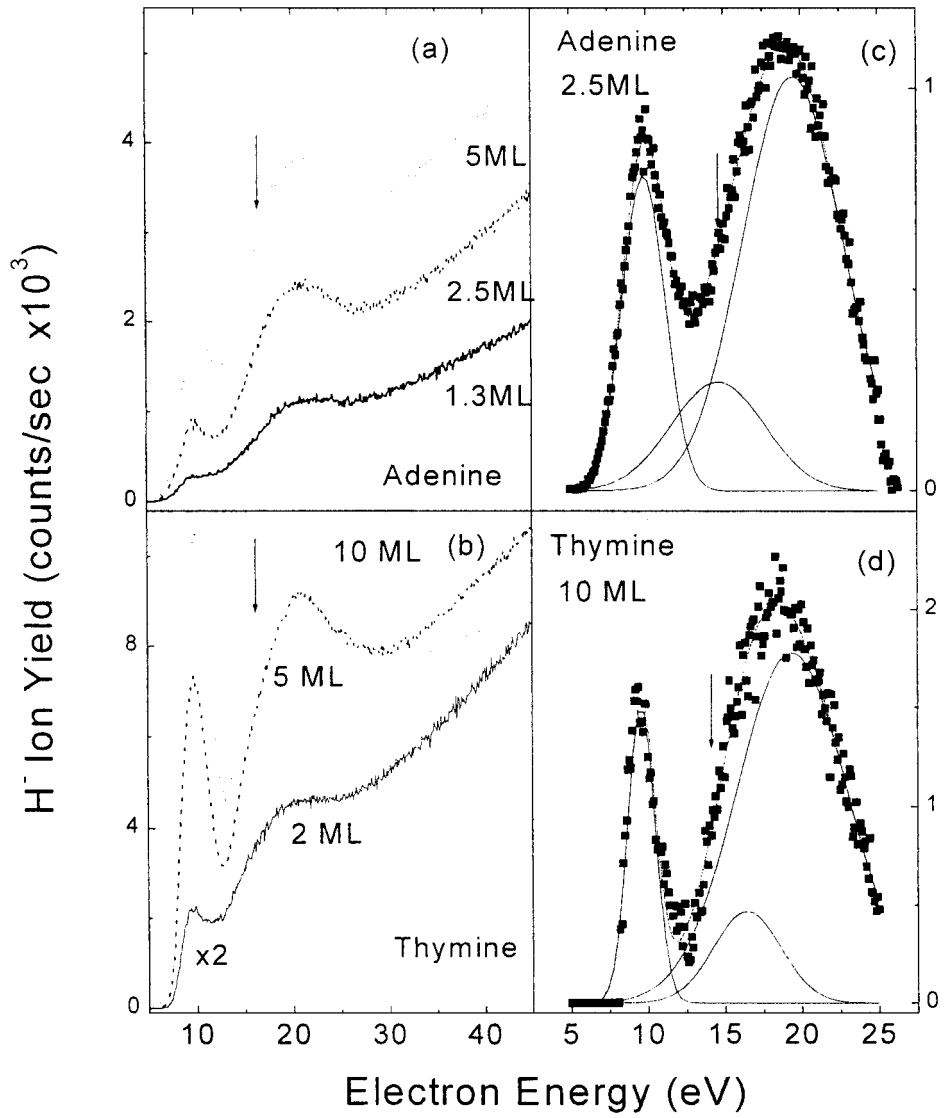

FIGURE 9. Electron-energy dependence of the H^- ion yield desorbed from (**a**) adenine and (**b**) thymine films of different thicknesses (in ML). The arrow indicates the shoulder observed at 14–15 eV incident electron energy. (**c**) Yield functions of adenine and (**d**) of thymine observed by subtracting a linear background from curves a and b, respectively. (Reprinted with permission from Abdoul-Carime, Cloutier, Sanche [2001]. Copyright 2001 Radiation Research.)

via, most likely, either stepwise (Andrieux, LeGorande, & Saveant, 1992) or concerted reactions (Stepanovic, Pariat, & Allan, 1999). The similarity of the CN^-, OH^-, and O^- ion-yield functions with resonant peaks at 9.0 and 10 eV from guanine or cytosine and thymine films, respectively, observed by Abdoul-Carime et al. (2001), suggests that they arise from the formation of a same excited isocyanic anion intermediate $(OCNH)^{*-}$, *via* closely lying but distinct resonances; i.e., (G^-, C^-, or T^-) $\rightarrow R^\bullet + (OCNH)^{*-}$, where $R^\bullet$ represents the remaining radical. $(OCNH)^{*-}$ further undergoes fragmentation into different possible dissociative channels: $CN^- + OH^\bullet$, $OH^- + CN^\bullet$, or $O^- + CNH^\bullet$.

D. Neutral-Species Desorption from Short Single-DNA Strands Induced by LEEs

In recent experiments, the damage produced by LEE impact on short single-strands of DNA was measured by ESD. Such a strand or oligonucleotide, consisting of three

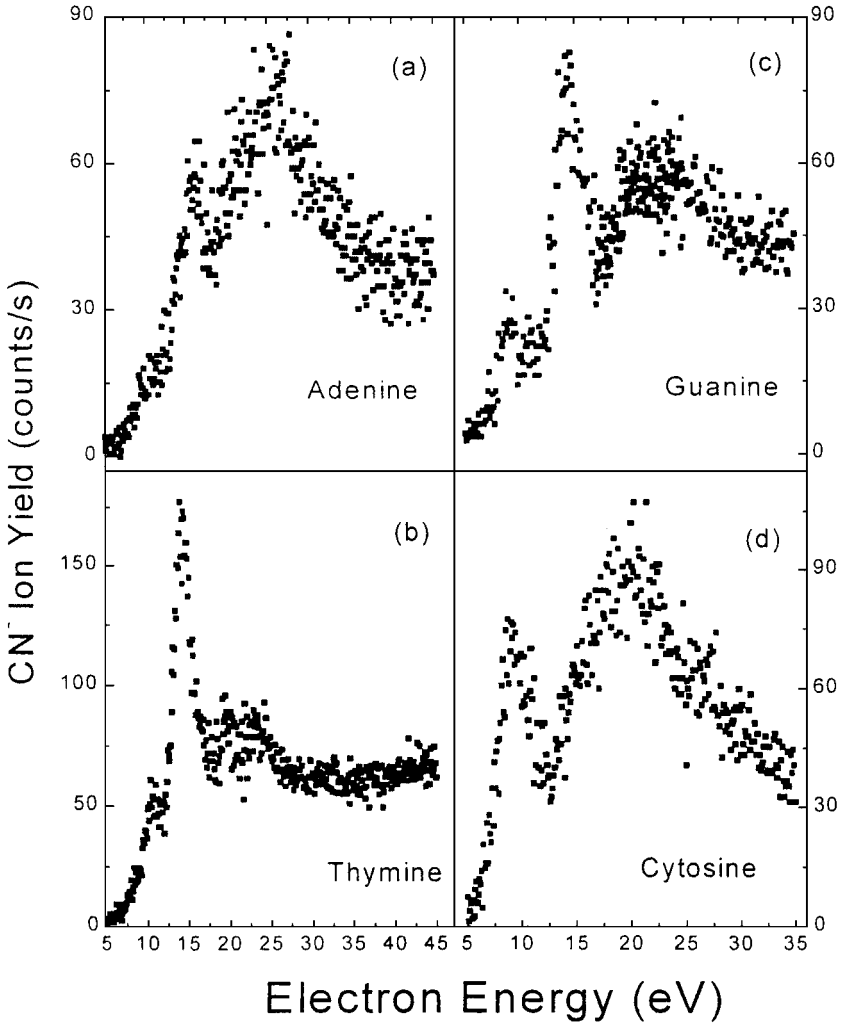

FIGURE 10. Incident-electron energy dependence of CN^- ion yields desorbed under 500 nA electron bombardment of 8-ML thick films of (**a**) Adenine, (**b**) Thymine, (**c**) Guanine, and (**d**) Cytosine. (Reprinted with permission from Abdoul-Carime, Cloutier, & Sanche [2001]. Copyright 2001 Radiation Research.)

base units, is shown in Figure 2b. Research in this area has been largely performed by Dugal et al. (1999, 2000) and Abdoul-Carime et al. (2000a,b, 2001, 2002), who measured the yields of neutral fragments induced by 1–30 eV electrons that impinged on oligonucleotides that consisted of 6 to 12 base units. The oligomers were chemisorbed on a gold surface *via* the sulfur-bonding technique described in Section II. Their results showed that LEE-impact dissociation of DNA bases led to the desorption of $CN^{\bullet}$, $OCN^{\bullet}$, and/or H_2NCN neutral species as the most intense observable yields. No sugar moieties were detected; nor were any phosphorus-containing fragments or entire bases. These results were obtained from mass spectrometric measurements, explained in Section II, of the residual atmosphere near the target during its bombardment in UHV by a 10^{-8} A electron beam. Figure 11 presents the electron-energy dependence of neutral $CN^{\bullet}$ (■) and $OCN^{\bullet}$ (and/or H_2NCN) (○) fragments desorbed per incident electron from oligomers that consist of nine bases (Abdoul-Carime, Dugal, & Sanche, 2000b; Dugal, Abdoul-Carime, & Sanche, 2000). The upper, middle, and lower panels show the results from oligonucleotides that consist of nine cytosine bases, Cy_9, six cytosine bases and three thymine bases, Cy_6T_3, and six cytosine bases and three bromouracil bases, Cy_6-BrU_3, respectively. The latter base is not naturally found in DNA, but it can be substituted for thymine and incorporated into cellular DNA, in place of thymine during DNA replication, to enhance the therapeutic effects of high-energy radiation (Zamenhof, De Giovanni, & Greer, 1958). Above 20 eV in Figure 11,

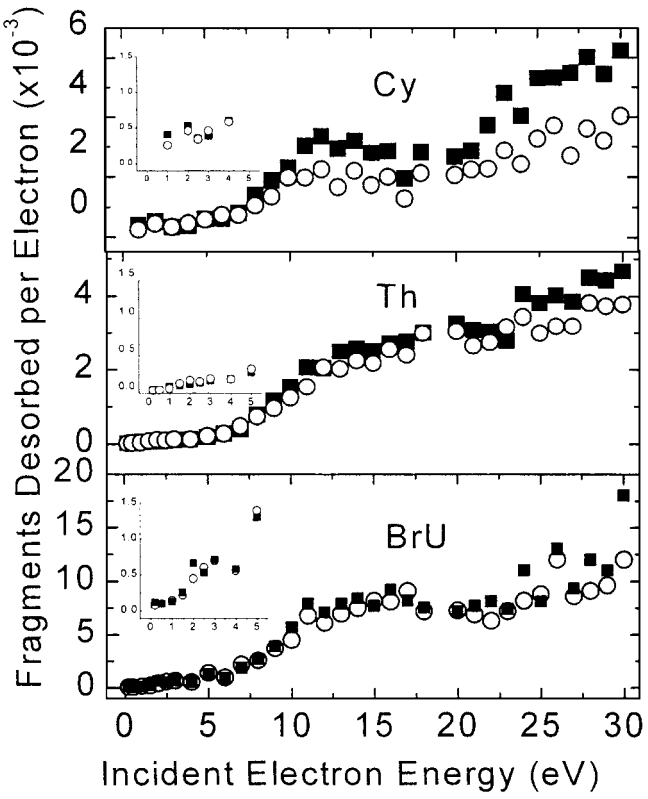

FIGURE 11. Incident-electron energy dependence of neutral CN (■) and OCN (and/or H_2NCN) (○) fragment desorption yields per incident electron from Cy_6-$(Cy)_3$ (**upper panel**), Cy_6-$(Th)_3$ (**middle panel**), and Cy_6-$(BrU)_3$ (**bottom panel**) oligonucleotides. The spread in the data is estimated to be 20%. (Reprinted with permission from Dugal et al. [2000]. Copyright 2000 American Chemical Society.)

the neutral-fragment production increases linearly with the incident-electron energy; that result is indicative of molecular fragmentation governed mostly by non-resonant dissociation and/or dissociative ionization of the bases (pathways a → a2 and/or c → c1 shown in Fig. 4). Below 20 eV, base fragmentation involves resonant and non-resonant excitation to dissociative electronic neutral states (pathways a → a2 and b → b2 → a2 in Fig. 4) and DEA (Dugal, Huels, & Sanche, 1999; Dugal, Abdoul-Carime, & Sanche, 2000a; Abdoul-Carime, Dugal, & Sanche, 2000b). The curves in Figure 11 present broad peaks, due to DEA, which are superimposed on a smoothly rising signal due to direct electronic excitation. At such relatively high energies (i.e., from 7 to 15 eV for all oligomers), the broad maxima are likely to reflect the formation of core-excited resonances that are dissociative in the Franck-Condon region. This interpretation is supported by: (1) the electron-energy losses in solid-phase DNA bases (Crewe, Isaacson, & Johnson, 1971) in the 7–15 eV range, which are attributed to the promotion of π- or σ-orbitals to higher energy ones; (2) the observation of resonant formation of H^- and CN^- at, respectively, 9–10 and 16 eV and 10–15 eV (e.g., Figs. 9 and 10) in the ESD yields from thin films of DNA bases (Herve du Penhoat et al., 2001; Abdoul-Carime, Cloutier, & Sanche, 2001a). Moreover, the threshold of neutral-species production that is observed at 5 eV coincides with the threshold for electronic excitations.

An extra peak is observed at 3 eV for BrU-substituted oligonucleotides in the inset at the bottom of Figure 11. Because this peak lies at an energy too low to involve any electronically excited states, it probably arises from the formation of a shape resonance that consists of the BrU molecule in the ground state with an electron that occupies a usually unfilled orbital. In XPS (Klyachko, Huels, & Sanche, 1999) investigations, LEE-induced damage to bromouracil was found to lead to a dissociation below 5 eV *via* resonant-electron capture by BrU followed by dissociation into a uracil-yl radical (U) and Br^-. The results were corroborated by measurements of the Br^- and U^- formation below 5 eV that was induced by electron impact of gaseous bromouracil (Huels et al., 1997; Abdoul-Carime et al., 2001). In a more detailed investigation of halogenated oligonucleotides (Dugal, Abdoul-Carime, & Sanche, 2000), it was further suggested that, after dissociation, BrU undergoes unimolecular dissociation that leads to the extrusion of an unstable OCNH moiety; afterwards, the latter dissociates to $CN^•$ and $OCN^•$. In such a case, the ratio of the yields of $CN^•$ and $OCN^•$ would be constant over a large energy range as seen in Figure 11.

E. Sequence-Specific Damage Induced by LEE Impact on Oligonucleotides

From various results, such as those shown in Figure 11, it has been possible to determine effective cross-sections or absolute desorption yields per base for base damage induced by LEE impact on homo-oligonucleotides (i.e., oligonucleotides that consist of only one type of base) (Dugal, Abdoul-Carime, & Sanche, 2000; Abdoul-Carime, Dugal, & Sanche, 2000b). As the strand length increased from 6 to 9 bases, a decrease in the yield per base was observed; that decrease was attributed to the greater probability of dissociation at the terminal bases (Abdoul-Carime, Dugal, & Sanche, 2000b; Abdoul-Carime & Sanche, 2001). Above nine units, no change larger than 5% of the signal was found. This percentage lies below experimental uncertainties, and the probability of fragmentation of a given base in an oligo can be considered to be constant in strands that contain ≥9 bases. Thus, these measurements provided an absolute determination of the chemical sensitivity of a base to LEE impact, in a nonamer or longer oligo that has the particular configuration provided by these experiments. With these absolute yields,

it became possible to calculate the expected yields for a specific hetero-oligonucleotide by simply adding the yield for each base contained in the strand. Such projected yields, for ≥ 9-mers oligonucleotides, necessarily assume that the damage is solely dependent on the chemical identity of the base, and does not depend on the environment of the base or sequence. Any different result found experimentally would thus indicate that the environment of the bases or their sequences play a role in DNA damage induced by LEE.

The incident electron-energy dependence of the projected (i.e., calculated) yields (Y) of $OCN^{\bullet}$ and $CN^{\bullet}$ per incident electron, desorbed from an hetero-oligonucleotide composed of six thymidine (T) and three deoxycitidine (dCy_9) units, is shown by the white squares in Figure 12. Each square represents, at a given electron energy, the yield $Y_{T6\text{-}dCy3} = 6Y_T + 3Y_{dCy}$, where 6 and 3 are the relative composition of DNA bases within the oligomer, and Y_T and Y_{dCy}, the yields per base for the respective homo-oligonucleotides. When the experiment is performed on such an hetero-oligonucleotide (i.e., 5′-TdCyTTdCyTTdCyT-3′), the curves represented by the black squares in Figure 12 for $OCN^{\bullet}$ and $CN^{\bullet}$ yields are obtained. If the DNA sequence had no effect, then the extrapolated curves would be, within experimental errors, identical to those measured experimentally. In contrast, when a protective effect occurs (i.e., less damage than expected is imparted to the bases), the white squares appear above the black squares and vice versa. For $CN^{\bullet}$ (Fig. 12b), we find, on average, a slight protective effect above 12 eV, which becomes more pronounced below that energy. For the production of $OCN^{\bullet}$ (Fig. 12a), the damage due to base sequence is even more dependent on energy: below 10 eV, protection is clearly observed, whereas at higher energies, cytosine substitution has a sensitizing effect (i.e., more damage than estimated is imparted). The strong peak observed around 12 eV in Figure 12a suggests that, at this resonance, the presence of cytosine promotes the production of $OCN^{\bullet}$. This strong enhancement of low-energy electron damage around 12 eV may be attributed to the sensitivity of the transient anion to its environment. It has been demonstrated, for small molecules such as O_2, that the lifetime of the intermediate anion (e.g., O_2^-) is sensitive to the chemical composition (Huels, Parenteau, & Sanche, 1994, 1997) and even the geometrical order of the environment (Bass et al., 2001). Because fragmentation occurs for dissociative anions that have a lifetime $\geq$one vibrational period along the relevant nuclear coordinates, DEA is strongly dependent on the lifetime of the intermediate anion. In fact, it has been suggested that changes in the sequence of a DNA strand affect the magnitude of DEA to the bases by modifying the lifetime of the base transient-anion (Abdoul-Carime & Sanche, 2001, 2002). Sequence sensitivity could also arise from an attack of adjacent bases by reactive radicals (Dugal, Abdoul-Carime, & Sanche, 2000) that is initiated through DEA to the nearby thymine or cytosine (Huels et al., 1997; Abdoul-Carime, Cloutier, & Sanche, 2001), leading to the extrusion of the isocyanic acid (OCNH), followed by dissociation into $OCN^{\bullet} + H^{\bullet}$ or $CN^{\bullet} + OH^{\bullet}$, as mentioned in Section IVD. The production of OCNH requires the scission of at least three C-N single bonds for cytosine, whereas only two are necessary for thymine. Thus, depending on the position of bases within the T_6-dCy_3 oligonucleotide, such secondary reactions through radicals are more effective with thymine than with cytosine.

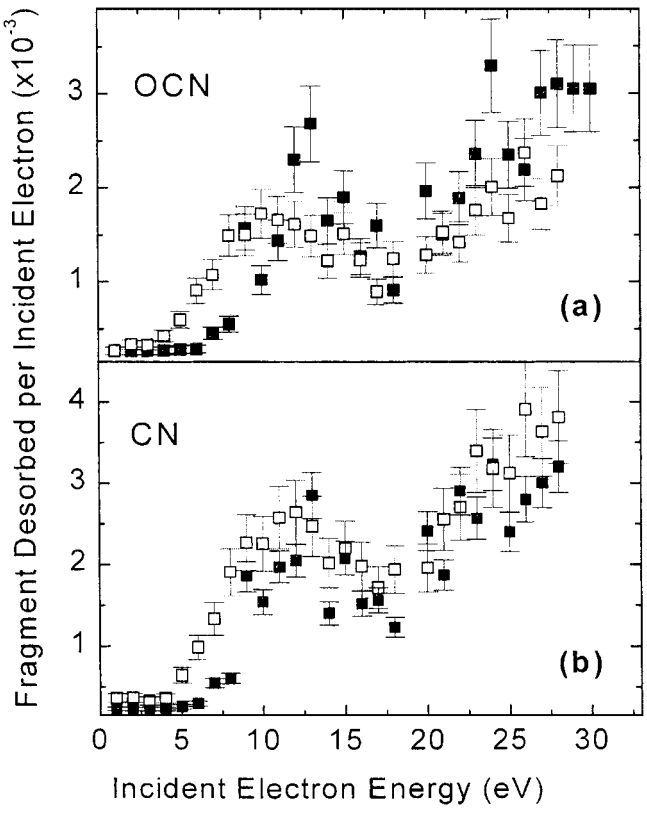

FIGURE 12. **Panels a** and **b** show the experimental (■) and extrapolated (□) values (see text) of the incident-electron energy dependence of the number of neutral OCN and CN fragments, respectively, desorbed per incident electron of 1–30 eV impinging on T_6-dCy_3 oligonucleotides; i.e., 5′-TdCyTTdCyTTdCyT-3′. The dashed curves are guides to the eye. The error bars lie within 15–20% of the plotted signal, and are the mean standard deviations of five data points. (Reprinted with permission from Abdoul-Carime & Sanche [2001]. Copyright 2001 Radiation Research.)

Further supporting evidence for sequence-dependent damage arises from measurements of $CH_3CCO^{\bullet}$ fragments, which are not detected with oligomers that contain only cytosine (Dugal, Huels, & Sanche, 1999; Abdoul-Carime, Dugal, & Sanche, 2000b). Over essentially the

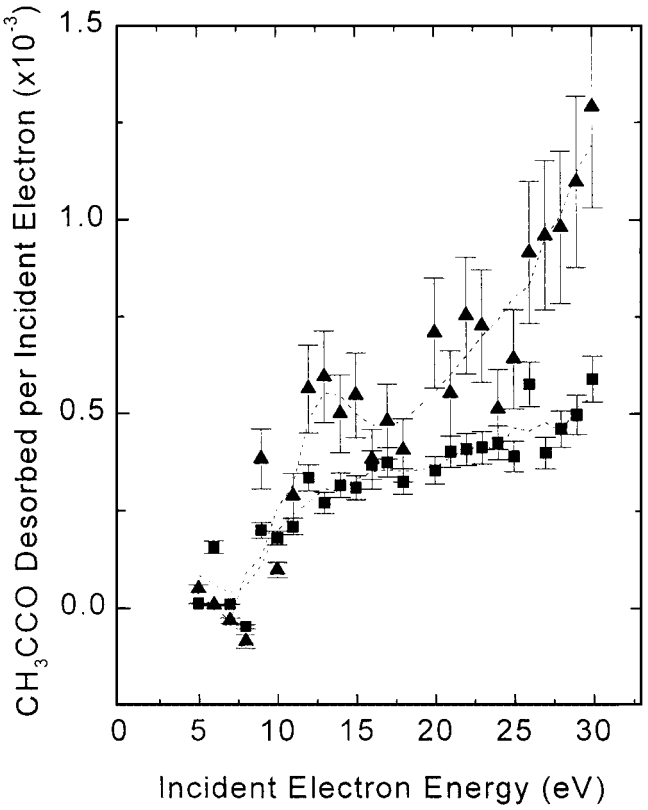

FIGURE 13. The CH_3CCO electron-stimulated desorption yield per incident electron, measured from T_9 (■) and T_6-dCy_3 (▲) oligonucleotides. The dashed curves are guides to the eye. The error bars represent a 15% variation of the data points, and are the mean standard deviations of five data points. (Reprinted with permission from Abdoul-Carime & Sanche [2001]. Copyright 2001 Radiation Research.)

entire energy range in Figure 13, the solid triangles, representing the yield of this fragment desorbed from T_6-dCy_3, lie above the solid squares, representing the yield from T_9, which has a density of thymine bases 50% higher than in the hetero-oligomer. In other words, even though $CH_3CCO^{\bullet}$ arises only from the dissociation of thymine, intercalating cytosine bases between the thymine units produces a surprisingly higher yield of $CH_3CCO^{\bullet}$ than that found with an oligomer composed of nine thymine units. This result provides clear evidence that this change in the molecular environment of thymine increases considerably the probability of its dissociation into $CH_3CCO^{\bullet}$ and the corresponding radical. In summary, the ensemble of the ESD results from oligonucleotides has shown that the sensitivity to LEE damage of a short single-DNA strand depends on the electron energy and the chemical nature of the bases as well as on the environment and the sequence of the bases.

F. Anion ESD from the Peptide and Disulfide Bridges of Proteins

Because the complexity of protein structure does not allow a direct detailed analysis of the mechanisms that underlie the fragmentation processes induced by LEE impact, recent research has first focused on the investigation of their action on protein sub-units and, more particularly, on the peptide and disufide bonds (Abdoul-Carime & Sanche, 2002b; Abdoul-Carime, Cecchini, & Sanche, 2002). These bonds can be modeled by acetamide (CH_3CONH_2) and dimethyl disulfide [$(CH_3S)_2$], respectively. Abdoul-Carime, Cecchini, & Sanche (2002) reported measurements of low-energy ESD of anions from acetamide and dimethyl disulfide (DMDS) films. Electron irradiation of physisorbed CH_3CONH_2 produces H^-, CH_3^-, and O^- anions, whereas the H^-, CH_2^-, CH_3^-, S^-, SH^-, and SCH_3^- anions are observed to desorb from DMDS films. Below 12 eV, the dependence of the anionic yields on the incident-electron energy exhibits structures that are indicative of fragmentation *via* DEA. Within the range 1–18 eV, (1.7 and

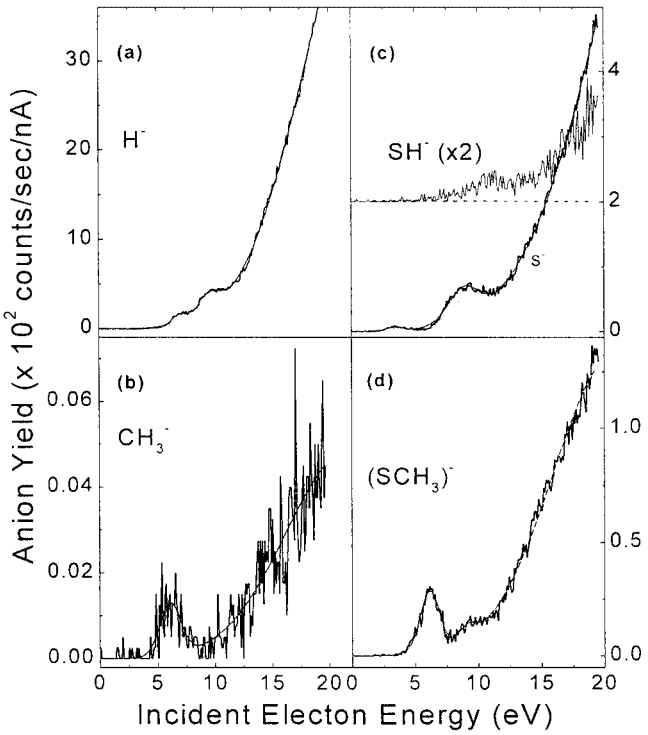

FIGURE 14. Electron-energy dependence of (**a**) H^-, (**b**) CH_3^-, (**c**) S^- and SH^-, and (**d**) (SCH_3) ion yields desorbed from low-energy electron bombardment of 3-ML thick dimethyl disulfide (DMDS) films. The SH^- yield function in **panel c** has been multiplied by a factor of 2. The smooth solid-line is the cumulative Gaussian fit to the data. Individual Gaussian functions are represented by dotted lines. (Reprinted with permission from Abdoul-Carime, Cecchini, & Sanche [2002]. Copyright 2002 Radiation Research.)

$1.4) \times 10^{-7}$ H^- ions/incident electron and (7.8×10^{-11} and 4.3×10^{-8}) of the other ions/incident electron desorb from acetamide and DMDS films, respectively. These results (Abdoul-Carime, Cecchini, & Sanche, 2002) suggest that, within proteins, the disulfide bond is much more sensitive to LEE attack than the peptide bond. The yield-functions for anion desorption from DMDS are shown in Figure 14. They were obtained by irradiating ~4-ML thick films with a 6.5 nA electron beam for H^- desorption and with an 8 nA beam for the heavier negative anions (Abdoul-Carime, Cecchini, & Sanche, 2002). The yield-functions exhibit structures at low energies, which are typical of DEA. A large portion of the anions that desorbed within the energy range of the peaks shown in Figure 14 are, therefore, produced through the first step of the reaction pathways suggested in Figure 15. According to those pathways, the resonant structures observed at 6.8 eV and 9.2 eV in the H^- yield function (Fig. 14a), arise from reaction E (Fig. 15), where a single bond ruptures at the methyl group. DEA to DMDS also induces a single sulfur-sulfur bond-cleavage through reaction B as shown by the production of $(SCH_3)^-$ anions. Within the lifetime of the transient anion $(CH_3SSCH_3)^-$, more complex exocyclic C-S ring cleavages, in addition to S-S bond breaks, may also lead to the formation of CH_3^-, S^-, and $(SH)^-$ and their neutral counterparts, as suggested by reactions A, C, and D in Figure 15. Reactions C and D may arise, *a priori*, through either simple bond-breaks or rearrangement reactions (Andrieux, LeGorande, & Saveant, 1992; Stepanovic, Pariat, & Allan, 1999). The latter process may occur when the lifetime of the negative precursor-ion is sufficiently long to sustain the deformation of molecular orbitals and substantial rearrangement of the nuclei.

The structure observed at similar energies in the $(CH_3)^-$ and $(SCH_3)^-$ anion yield-functions in Figure 14 suggests competitive channels for transient $(CH_3SSCH_3)^{*-}$ dissociation at approximately 6.0 eV. Competitive fragmentation may also occur at ~9.0 eV for that of H^-, S^-, and $(SCH_3)^-$. At these energies, the incoming electron is likely to transfer energy to electronically excite a target molecule and to be captured by the positive electron-affinity of the excited state. Thus, the formation of stable negative ions is likely to occur *via* a dissociation of core-excited resonances. Above 12 eV, nonresonant DD dominates the production of anion fragments. As seen by the quasi-linear rise of the signal in this region in Figure 14, the anion yield-functions exhibit a typical monotonic increase with the energy of the incoming free electron, as a result of the excitation of neutral CH_3SSCH_3 molecules to a dissociative electronic excited state, whose dissociation limit consists of the stable anions represented in Figure 15 and the corresponding cation.

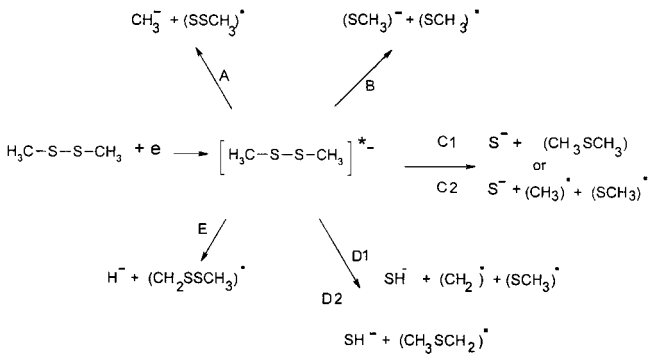

FIGURE 15. Possible dissociation pathways (**a–e**) for stable anion production after low-energy electron attachment to physisorbed DMDS. All negative ions represented were observed to desorb under electron bombardment of DMDS films. (Reprinted with permission from Abdoul-Carime, Cecchini, & Sanche [2002]. Copyright 2002 Radiation Research.)

G. LEE Damage to Plasmid DNA

Boudaiffa et al. bombarded, with 3 eV to 1.5 keV electrons, pure dry samples of plasmid DNA films (Boudaiffa et al., 2000a,b,c, 2002; Huels et al., submitted), which afterwards were analyzed according to the procedure described in Section IIC. By measuring the relative quantities of the various forms of DNA in their 5-ML sample as a function of exposure to 10, 30, and 50 eV electrons, these authors measured the total effective cross-section ($\sim 4 \times 10^{-15}$ cm^2) and effective range (~13 nm) for the destruction of supercoiled DNA, at these energies (Boudaiffa et al., 2002). Such experiments also allowed Boudaiffa et al. to delineate the regime under which the measured yields were linear with electron exposure. It is within this regime that the incident electron energy dependence of damage to DNA was recorded more continuously between 3 and 100 eV (Boudaiffa et al., 2000a,c; Huels et al., submitted). The most striking observations were that: (1) these yields did not depend on the ionization cross-section, and (2) below 15 eV, the yields varied considerably with incident electron energy. Above 20 eV, the yields of SSB and DSB did not exhibit any pronounced energy variations, nor did they increase considerably with increasing energy.

The incident-electron energy dependence for the formation of at least one SSB and a DSB in supercoiled DNA is shown in Figure 16. These curves were recorded in the linear regime. Thus, each SSB or DSB represented in Figure 16 is the result of a single-electron interaction. The data indicate that LEE-induced damage is highly dependent on the initial kinetic energy, particularly below 15 eV, with thresholds near 3 to 5 eV and intense peaks near 10 eV. These yield functions can be understood from the results of the fragmentation induced by LEE to the various sub-units of the DNA molecule reported in this section, including its

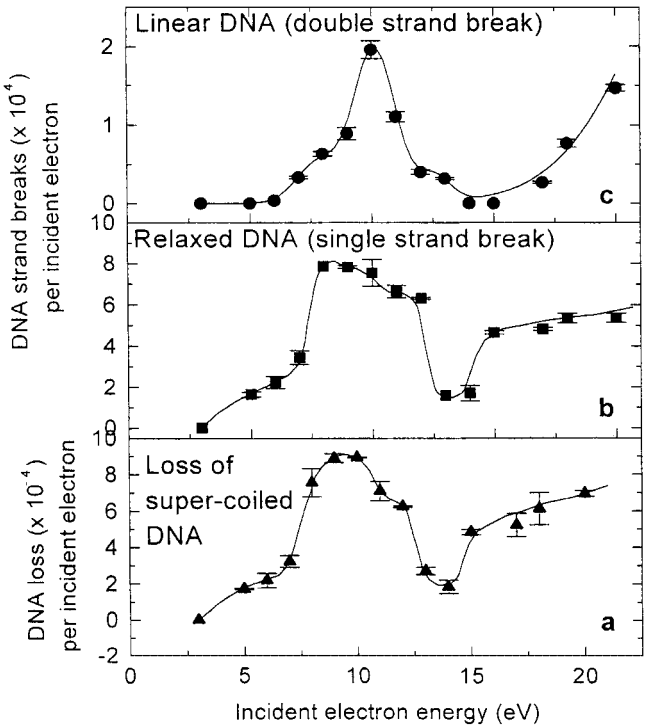

FIGURE 16. Measured yields, per incident electron of 3–20 eV, for the induction of DSBs (**a**), SSBs (**b**), and loss of the supercoiled DNA form (**c**) in dry DNA films. The error bars correspond to one standard deviation from six measurements. (Reprinted with permission from Boudaiffa et al., Science 287:1658–1660, 2000a. Copyright 2000 American Association for the Advancement of Science.)

structural water; as shown in this article, the incident-electron energy dependence of the damage to elementary constituents of DNA, probed in the form of desorbed anions and neutral species, exhibits strong variations due to electron resonances. From comparison of the maxima in the anion- and neutral-desorption yield-functions of these DNA constituents to the DNA results, it becomes quite obvious that the strong energy dependence of the DNA strand breaks below 15 eV in Figure 16 can be attributed to the initial formation of transient anions, decaying into the DEA and/or dissociative electronic excitation channels exemplified in Figure 4. However, because the basic DNA components (i.e., the sugar and base units and structural H_2O) can all be fragmented *via* DEA between 5 and 13 eV, it is not possible to unambiguously attribute SSBs and DSBs to the initial dissociation of a specific component. For example, the maximum in the SSB yield that lies near 8 eV is very close to the maximum in $H^- + OH$ production from H_2O (Fig. 5), but the DNA bases also produce H^- and the corresponding radical with high efficiency near 9 eV (Fig. 9). What appears to be more convincing is the coincidence in the 10 eV peak in H^- production in Figure 8 from tetrahydrofuran and its analogs, with that in the DSB yield seen in Figure 16. This result is not surprising, because two events are necessary to create a DSB, and the probability for such breaks is likely to be larger when the first hit results in a SSB (i.e., in a break on the sugar-phosphate backbone). Another interesting aspect of the DSB yield-curve is the absence of damage induced by direct (non-resonant) electronic transitions. Indeed, the two points in Figure 16 around 14 and 15 eV lie at the zero baseline, indicating that, below ~16 eV, DSB occurs exclusively *via* the decay of transient anions. These observations suggest that, below ~16 eV, DSB occurs *via* molecular dissociation on one strand initiated by the decay of a transient anion, followed by reaction of at least one of the fragmentation products on the opposite strand (Boudaiffa et al., 2000a,c). This hypothesis is further supported by the observation of electron-initiated fragment reactions (such as hydrogen abstraction, dissociative charge-transfer, atom- and functional-group exchange, and reactive scattering) that occur over distances comparable to the DNA double-strand diameter (~2 nm) in condensed films that contain water or small linear and cyclic hydrocarbons (Huels, Parenteau, & Sanche, 1997; Bass et al., 1998; Sieger, Simpson, & Orlando, 1998).

Within cells, histones and the other chromosomal proteins are in close contact with DNA. It is, therefore, possible that the radicals produced from secondary LEE, generated by high-energy radiation, may not only denature proteins, as suggested by the results of the previous subsection, but may also induce reactions with nearby nucleic acids and, therefore, damage DNA. Thus, in future experiments, films composed of DNA and proteins should be investigated in order to mimic more closely the action of LEE in biological cells.

V. SUMMARY AND CONCLUSIONS

Recent results on the damage induced by low-energy electrons to DNA, some of the basic constituents of DNA, and protein subunits have been reviewed in this article. At low energies, the incident-electron energy dependence of the yield of anions desorbed from films of these constituents (e.g., water ice, deoxyribo analogs, dimethyl disulfate, and DNA bases) exhibits strong variations that are typical of dissociative electron attachment to these molecules. Above 12–15 eV, the monotonic increase with energy in the desorbed anion yields is typical of non-resonant dipolar dissociation. The latter process and dissociative ionization can also lead to cation desorption from electron-bombarded films—as shown for the case of electron-stimulated desorption of protons from water-ice films. Structures in the incident-electron energy dependence of the yield of neutral radicals desorbed from

solid H_2O films and oligonucleotides chemisorbed on gold can also be interpreted to arise from the dissociation of transient anions or their decay into dissociative electronic states. The results obtained with homo- and hetero-oligonucleotides indicate that damage to short DNA strands by 1–30 eV electrons is affected by base substitution. The modification of induced damage is due to the chemical nature of the bases, as well as to their environment and/or sequence. These findings reinforce the idea (Fuciarelli et al., 1994; Sy et al., 1997) that genomic sensitivity to ionizing radiation depends on local genetic information. Combined with the results on slow-electron damage to DNA and its components, reviewed in this article, these results further suggest that such a sensitivity may arise, at least partially, from the specific action of low-energy (3–30 eV) electrons that are generated in large amounts by the primary ionizing particles.

In Section IVG, the results obtained with the basic constituents of DNA were compared to the measured yields per incident electron for the induction of SSB and DSB in supercoiled DNA by the impact of 3–20 eV electrons. Such a comparison shows that, below 15 eV, the DNA damage results principally from the formation of transient molecular anions localized on the DNA's basic components. These transitory states arise from the fundamental electrodynamic and exchange forces that act between the electron and a specific sub-unit of the DNA. Because of their universality, these fundamental interactions are expected to also operate in living cells. Thus, from a radiobiological perspective, the results summarized in this article suggest that the abundant low-energy secondary electrons, and possibly their ionic and radical reaction products, play a crucial role in the nascent stages of cellular DNA radiolysis and may already induce substantial damage long before their thermalization along ionizing radiation tracks.

ACKNOWLEDGMENTS

The author thanks Ms. Francine Lussier, L. Parenteau, and Dr. Andrew D. Bass in the preparation of this manuscript, and Dr. Darel Hunting for discussions and helpful comments.

REFERENCES

Abdoul-Carime H, Cecchini S, Sanche L. 2002. Alteration of protein structure induced by low-energy (<18 eV) electrons: I. The peptide and disulfide bridges. Radiat Res 158:23–31.

Abdoul-Carime H, Cloutier P, Sanche L. 2001. Low energy (5–40 eV) electron stimulated desorption of anions from physisorbed DNA bases. Radiation Res 155:625–633.

Abdoul-Carime H, Dugal PC, Sanche L. 2000a. Damage induced by 1–30 eV electrons on thymine and bromouracil substituted oligonucleotides. Radiation Res 153:23–28.

Abdoul-Carime H, Dugal PC, Sanche L. 2000b. DIET of neutral fragments from chemisorbed biological molecular systems. Surf Sci 451:102–107.

Abdoul-Carime H, Sanche L. 2001. Sequence specific damage to oligonucleotides induced by 3–30 eV electrons. Radiat Res 156:151–157.

Abdoul-Carime H, Sanche L. 2002a. Fragmentation of short single DNA strands by 1–30 eV electrons: Dependence on base identity and sequence. Int J Radiat Biol 78:89–99.

Abdoul-Carime H, Sanche L. 2002b. Mechanisms for anion and sulfur-radical production by 1–18 eV electron impact on dimethyl disulfur adsorbed on ice. J Phys Chem B 106: 12186–12190.

Abdoul-Carime H, Huels MA, Illenberger E, Sanche L. 2001. Sensitizing DNA to secondary electron damage: Resonant formation of oxidative radicals from 5-Halouracils. JACS 123:5354–5355.

Allan M. 1989. Study of the triplet-states and short-lived negative-ions by means of electron impact sceptroscopy. J Electr Spectr Rel Phenom 48:219–351.

Andrieux CP, LeGorande A, Saveant J-M. 1992. Electron transfer and bond breaking–examples of passage from a sequential to a concerted mechanism in the electrochemical reductive cleavage of arylmethyl halides. J Amer Chem Soc 114: 6892–6904.

Antic D, Parenteau L, Sanche L. 2000. Electron stimulated desorption of H^- from condensed phase deoxyribose analogs: Dissociative electron attachment vs. resonance decay into dipolar dissociation. J Phys Chem B 104:4711–4716.

Antic D, Parenteau L, Lepage M, Sanche L. 1999. Low energy electron damage to condensed phase deoxyribose analogs investigated by electron stimulated desorption of H^- and electron energy loss spectroscopy. J Phys Chem 103:6611–6619.

Bass AD, Parenteau L, Huels MA, Sanche L. 1998. Reactive scattering of O^- in organic films at sub-ionization collision energies. J Chem Phys 109:8635–8643.

Bass AD, Parenteau L, Weik F, Sanche L. 2001. Effects of morphology on the low-energy electron stimulated desorption of O^- from O_2 deposited on benzene and water ices. J Chem Phys 115:4811–4818.

Bennett SL, Greenwood CL, Williams EM, de Segovia JL. 1991. Evidence of multiple H^+ ion desortion pathways with ESD of chemisorbed and multilayer water. Surf Sci 251(252): 857–860.

Bertel E, Ramaker DE, Kurtz RL, Stockbauer R, Madey TE. 1985. Photon stimulated desorption of H^+ ions from OH on Ti and Cr—Comparison with bulk solid H_2O. Phys Rev B 31:6840–6842.

Boudaiffa B, Cloutier P, Hunting D, Huels MA, Sanche L. 2000a. Resonant induction of DNA strand breaks by low energy (3–20 eV) electrons. Science 287:1658–1660.

Boudaiffa B, Hunting DJ, Cloutier P, Huels MA, Sanche L. 2000b. Induction of single and double strand breaks in plasmid DNA by 100 to 1500 eV electrons. Int J Radiat Biol 76:1209–1221.

Boudaiffa B, Cloutier P, Hunting D, Huels MA, Sanche L. 2000c. Les électrons de très faible énergie produisent des lésions de l'ADN. Méd Sci 16:1281–1283.

Boudaiffa B, Cloutier P, Hunting D, Huels MA, Sanche L. 2002. Cross-sections for low-energy (10–50 eV) electron damage to DNA. Radiat Res 157:227–234.

Christophorou LG. 1984. Electron-molecule interactions and their applications. Orlando: Academic Press.

Cobut V, Frongillo Y, Patau JP, Goulet T, Fraser M-J, Jay-Gerin J-P. 1998. Monte Carlo simulation of fast electron and proton tracks in liquid water-I. Physical and physicochemical aspects. Radiat Phys Chem 51:229–243.

Crewe AV, Isaacson M, Johnson D. 1971. Electron energy loss spectrum of nucleic-acid bases. Nature 231:262–264.

Dillon MA, Tanaka H, Spence D. 1989. The electronic spectrum of adenine by electron-impact methods. Radiat Res 117:1–7.

Ding MQ, Williams EM, Adrados JP, de Segovia JL. 1984. Energy distribution of H^+ ions with ESD of water adsorbed at aluminum and tungsten surfaces. Surf Sci Lett 14:L264–L268.

Dugal P, Abdoul-Carime H, Sanche L. 2000. Mechanisms of low energy (0.5–30 eV) electron-induced pyrimidine ring fragmentation within thymine and halogen-substituted single strands of DNA. J Phys Chem B 104:5610–5617.

Dugal P, Huels MA, Sanche L. 1999. Low-energy (5–25 eV) electron damage to homo-oligonucleotides. Radiation Res 151:325–333.

Fuciarelli AF, Sisk EC, Miller JH, Zimbrick JD. 1994. Radiation induced electron migration in nuclic-acids. Int J Radiat Biol 66:505–509.

Herve du Penhoat MA, Huels MA, Cloutier P, Jay-Gerin JP, Sanche L. 2001. Electron stimulated desorption of H^- from thin films of thymine and uracil. J Chem Phys 114:5755–5764.

Hoffman A, Laikhtman A, Ustaze S, Hadj Hamou M, Hedhili MN, Guillotin J-P, Le Coat Y, Teillet Billy D, Azria R. 2001. Dissociative electron attachment and dipolar dissociation of H^- electron stimulated desorption from hydrogenated diamond films. Phys Rev B 63:45401–45408.

Huels MA, Parenteau L, Sanche L. 1994. Substrate dependence of electron-stimulated O^- yields from dissociative electron attachment to physisorbed O_2. J Chem Phys 100:3940–3956.

Huels MA, Parenteau L, Sanche L. 1997. Substrate sensitivity of dissociative electron attachment to physisorbed aniline. Chem Phys Lett 279:223–229.

Huels MA, Boudaïffa B, Cloutier P, Hunting D, Sanche L. Submitted.

Huels MA, Parenteau L, Michaud M, Sanche L. 1995. Kinetic-energy distributions of O^- produced by dissociative electron attachment to physisorbed O_2. Phys Rev A 51:337–349.

Huels MA, Hahndorf I, Illenberger E, Sanche L. 1998. Resonant dissociation of DNA bases by sub-ionization electrons. J Chem Phys 108:1309–1312.

Inokuti M. 1991. How is radiation energy-absorption different between the condensed phase and gas phase. Radiat Eff Def Sol 117:143–162.

International Commission on Radiation Units and Measurements. 1979. ICRU Report 31. ICRU, Washington DC .

Kimmel GA, Orlando TM. 1995. Low-energy (5–120 eV) electron-stimulated dissociation of amorphous D_2O ice-D(S-2), O(P-3(2,1,0)), and O(D-1(2)) yields and velocity distributions. Phys Rev Lett 75:2606–2609.

Kimmel GA, Orlando TM. 1996. Observation of negative ion resonances in amorphous ice via low-energy (5–40 eV) electron-stimulated production of molecular hydrogen. Phys Rev Lett 77:3983–3986.

Kimmel GA, Orlando TM, Vézina C, Sanche L. 1994. Low-energy electron-stimulated production of molecular hydrogen from amorphous water ice. J Chem Phys 101: 3282–3286.

Kimmel GA, Orlando TM, Cloutier P, Sanche L. 1997. Low-energy (5–40 eV) electron stimulated desorption of atomic hydrogen and metastable emission from amorphous ice. J Phys Chem 101:6301–6308.

Klyachko DV, Huels MA, Sanche L. 1999. Halogen anion formation in 5-halo-uracil films: X rays vs. subionization electrons. Radiation Res 151:177–187.

Langenbach E, Spitzer A, Luth H. 1984. The adsorption of water on Pt(111) studied by IR-Reflection and UV-Photoemission spectroscopy. Surf Sci 147:179–190.

LaVerne JA, Pimblott SM. 1995. Electron energy-loss distributions in solid, dry DNA. Radiat Res 141:208–215.

Lorentzon J, Fulsher MP, Roos BO. 1995. Theoretical study of the electronic spectra of uracil and thymine. J Am Chem Soc 117:9265–9273.

Marsolais RM, Deschênes M, Sanche L. 1989. Low energy electron transmission method for measuring charge trapping in dielectric films. Rev Scient Instr 60:2724–2732.

Massey HSW. 1976. Negative ions. London: University Press.

Mely B, Pullman A. 1969. Ab initio calculations on cytosine, thymine and adenine. Theor Chim Acta 13:278–284.

Mott NF, Massey HSW. 1965. The theory of atomic collisions. Oxford: Claren-don.

Noell JO, Melius CF, Stulen RH. 1985. Mechanism of electron stimulated desorption of protons from water-gas chemisorbed and ice phases. Surf Sci 157:119–150.

Nyberg M, Hasselström J, Karis O, Wassdahl N, Weinelt M, Nilsson A, Petterson LGM. 2000. The electronic structure and surface chemistry of glycine adsorbed on Cu(110). J Chem Phys 112:5420–5427.

Palmer RE, Rous P. 1992. Resonances in electron-scattering by molecules on surface. Rev Mod Phys 64:383–440.

Patthey L. 1995. Ph.D. thesis, Université de Lausanne .

Porter MD, Bright TB, Allara DL, Chidsey CED. 1987. Spontaneously organized molecular assemblies: 4. Structural

characterization of normal alkyl thiol monolayers on gold by optical ellipsometry infrared spectroscopy and electrochemistry. J Am Chem Soc 109:3559–3568.

Rakhovskaia O, Wiethoff P, Feulner P. 1995. Thresholds for electron stimulated desorption of neutral molecules from solid N_2, CO, O_2 and NO. Nucl Instrum Methods B 101: 169–173.

Rosenberg RA, LaRoe PR, Rehn V, Stohr J, Jaeger R, Parks CC. 1983. K-shell excitation of D_2O and H_2O ice, photoion and photoelectron yields. Phys Rev B 28:3026–3030.

Rowntree P, Parenteau L, Sanche L. 1991. Electron stimulated desorption via dissociative attachment in amorphous H_2O. J Chem Phys 94:8570–8576.

Sanche L. 1991. Primary interactions of low-energy electrons in condensed matter. In: Jay-Gerin J-P, Ferradini C, editors. Excess electrons in dielectric media. Boca Raton: CRC Press. p 1–42.

Sanche L. 1995. Interaction of low-energy electrons with atomic and molecular solids. Scanning Microsc 9:619–656.

Sanche L. 2000. Electron resonances in desorption induced by electronic transitions. Surf Sci 451:82–90.

Sanche L, Deschênes M. 1988. Mechanisms of charge trapping at a dielectric surface. Phys Rev Lett 61:2096–2098.

Schulz GJ. 1973. Resonances in electron impact on atoms. Rev Mod Phys 45:378–422 ; resonances in electron impact on diatomic molecules. ibid 45:423–486.

Sieger MT, Simpson WC, Orlando TM. 1997. Electron-stimulated desorption of D^+ from D_2O ice-surface structure and electronic excitations. Phys Rev B 56:4925–4937.

Sieger MT, Simpson WC, Orlando TM. 1998. Production of O_2 on icy satellites by electronic excitation of low-temperature water ice. Nature 394:554–556.

Simpson WC, Sieger MT, Orlando TM, Parenteau L, Nagesha K, Sanche L. 1997. Dissociative electron attachment in nanoscale ice films: Temperature and morphology effects. J Chem Phys 107:8668–8677.

Simpson WC, Orlando TM, Parenteau L, Nagesha K, Sanche L. 1998. Dissociative electron attachment in ice films: Thickness and charge trapping effects. J Chem Phys 108:5027–5034.

Srdoc D, Inokuti M, Krajcar-Bronic I, Waibel E, Hatano Y, Kaplan I. 1995. In: Inokuti M , editor. Atomic and molecular data for radiotherapy. IAEA CRP, Vienna. p 547–609.

Stepanovic M, Pariat Y, Allan M. 1999. Dissociative electron attachment in cyclopentanone, gamma-butyrolactone, ethylene carbonate, and ethylene carbonate-d(4): Role of dipole-bound resonances. J Chem Phys 110:11376–11382.

Stockbauer R, Hanson DM, Flodstrom SA, Madey TE. 1982. Photon stimulated desorption and ultraviolet photoemission spectroscopic study of the interaction of H_2O with a Ti(001) surface. Phys Rev B 26:1885–1892.

Stulen RH, Thiel PA. 1985. Electron stimulated desorption and thermal desorption spectroscopy of H_2O on nickel(111). Surf Sci 157:99–118.

Suzuki M. 1990. The heptad repeat in the largest subunit of RNA polymerase II binds by intercalating into DNA. Nature 344:562–565.

Sy D, Savoie C, Begusova B, Michalik V, Charlier M, Spotheim-Maurizot M. 1997. Sequence-dependent variations of DNA structure modulate radiation-induced strand breakage. Int J Radiat Biol 72:147–155.

Takayanagi K. 1967. Scattering of slow electrons by molecules. Prog Theor Phys Suppl Jpn 40:216–248.

von Sonntag C. 1987. The chemical basis for radiation biology. London: Taylor and Francis.

Ward JF. 1977. Advances in radiation biology, Vol. 5. New York: Academic Press .

Werner MH, Clore GM, Fisher CL, Fisher RJ, Trinh L, Shiloach J, Gronenborg AM. 1995. The solution structure of the human ETS1-DNA complex reveals a novel mode of binding and true side chain intercalation. Cell 83:761–771.

Yamamoto O. 1976. Aging carcinogenesis and radiation biology. New York: Plenum.

Yu C, Peng S, Akayama I, Lin J, LeBreton PR. 1978. Ultraviolet photoelectron studied of biological pyrimidines—Valence electronic-structure of cytosine. J Am Chem Soc 100:2303–2307.

Zamenhof S, De Giovanni R, Greer S. 1958. Induced gene unstabilization. Nature 181:827–829.